



UvA-DARE (Digital Academic Repository)

Photonic Kondo-like model

Pletyukhov, M.; Müller, N.; Gritsev, V.

Published in:
Physical Review A

DOI:
[10.1103/PhysRevA.95.043829](https://doi.org/10.1103/PhysRevA.95.043829)

[Link to publication](#)

Citation for published version (APA):
Pletyukhov, M., Müller, N., & Gritsev, V. (2017). Photonic Kondo-like model. *Physical Review A*, 95(4), [043829].
<https://doi.org/10.1103/PhysRevA.95.043829>

General rights

It is not permitted to download or to forward/distribute the text or part of it without the consent of the author(s) and/or copyright holder(s), other than for strictly personal, individual use, unless the work is under an open content license (like Creative Commons).

Disclaimer/Complaints regulations

If you believe that digital publication of certain material infringes any of your rights or (privacy) interests, please let the Library know, stating your reasons. In case of a legitimate complaint, the Library will make the material inaccessible and/or remove it from the website. Please Ask the Library: <https://uba.uva.nl/en/contact>, or a letter to: Library of the University of Amsterdam, Secretariat, Singel 425, 1012 WP Amsterdam, The Netherlands. You will be contacted as soon as possible.

Photonic Kondo-like modelMikhail Pletyukhov,¹ Niclas Müller,¹ and Vladimir Gritsev²¹*Institute for Theory of Statistical Physics and JARA–Fundamentals of Future Information Technology, RWTH Aachen University, 52056 Aachen, Germany*²*Institute for Theoretical Physics, Universiteit van Amsterdam, Science Park 904, Postbus 94485, 1098 XH Amsterdam, The Netherlands*

(Received 30 November 2016; published 20 April 2017)

We introduce and study a photonic analog of the Kondo model. The model is defined as a far-detuned regime of photonic scattering off a three-level emitter in a Λ -type configuration coupled to a one-dimensional waveguide with linear dispersion. We study dynamics of this local emitter driven by a coherent field pulse as well as the first- and second-order correlation functions of a scattered light. Various polarization-dependent correlation effects and an entanglement between the emitter and transmitted photons are quantified by the purity of an emitter's state. We also show that statistical properties of the scattered light are very sensitive to a polarization of the incoming coherent pulse.

DOI: [10.1103/PhysRevA.95.043829](https://doi.org/10.1103/PhysRevA.95.043829)**I. INTRODUCTION**

In recent years, there have been many theoretical proposals and partial experimental realizations which aimed to bridge the interface between condensed-matter physics and quantum optics. The objectives of these proposals are twofold. Some of them are triggered by ideas of quantum simulation of quantum many-body condensed-matter models using the tools of quantum optics while the others were inspired by advances in quantum information, since the eventual scalability of quantum architecture would inevitably introduce some many-body aspects into quantum optical dynamics.

On the quantum simulation side, these proposals include, in particular, the Bose-Hubbard model of Mott-superfluid transition for polaritons [1–3], one-dimensional physics leading to a photonic fermionization [4,5], Bose condensation of light [6], topological photonic states [7,8], and quantum Hall fluids for photons [9]. For a review, see Refs. [10,11].

On the quantum information and computation side, the main player is the entanglement which requires the presence of interaction between elements of quantum networks with a simultaneous protection against an action of the environment [12]. In this respect, several proposals of hybrid systems are considered as the most promising route for realizing future functional devices. The role of qubits in these schemes are played by real or artificial atoms (e.g., quantum dots) or other solid-state based structures (e.g., nitrogen-vacancy centers; for a review, see Ref. [13]), while the information is transferred between them by photons or other (sometimes collective) excitations (e.g., polaritons). To ensure efficient functionality, qubits must be entangled in a controllable way. Entanglement can be encoded into either polarization degrees of freedom of photons or some collective degrees of freedom, and can be shared with internal degrees of freedom of a qubit, thus producing the qubit-field entanglement which may then be transferred to a different qubit of a device by photons. This philosophy has been successfully realized in several recent experiments, thus achieving qubit-qubit entanglement for distances ranging from nanometers to kilometers [14–17].

From a more general perspective, multilevel schemes exhibit a variety of linear and nonlinear properties built in by quantum interference phenomena between different quantum level pathways. This includes electromagnetically

induced transparency [18,19], coherent population trapping [20–25], stimulated Raman adiabatic passage (STIRAP) [26–30], Autler-Townes effect [31–33], resonance fluorescence [34–42], controllable Kerr nonlinearity [43–45], and two-photon fluorescence [46,47]. In addition, the role of a photonic polarization essentially increases in the Raman and magneto-optical effects [48].

Here we present a model which, on one hand, extends the list of proposals for photonic quantum simulators and, on the other hand, can be used for quantum information purposes as an interface for photon-qubit entanglement transfer. This model bears a number of similarities with the Kondo model known in condensed-matter physics, while many important differences remain because of Bose statistics of photons. With these differences in mind, we call it a *photonic Kondo-like model*, in analogy with the fermionic Kondo model. The electronic Kondo model, as introduced by Kondo in 1964 [49], describes the interaction of a reservoir of electrons coupled to a quantum impurity modeled by a local spin- $\frac{1}{2}$ system. It was proposed to account for a nonmonotonous behavior of the resistivity in certain metallic alloys containing small concentrations of magnetic impurities at low temperatures. The model can, in a certain limit, be derived from the Anderson model [50]. Later on, it has been extended to problems of nonequilibrium electronic transport through quantum dots [51,52]. From the quantum optical point of view, the ideology of impurity models is quite natural, since localized quantum optical emitters resemble local impurity spins of condensed-matter models, while propagating photons are the analogues of itinerant electrons in solids.

Our model is realized by a three-level Λ scheme (see Fig. 1), where single-photon transitions $|+\rangle \leftrightarrow |3\rangle$ and $|-\rangle \leftrightarrow |3\rangle$ are only coupled to photons of left ($\sigma = -$) and right ($\sigma = +$) polarizations, respectively. The direct $|+\rangle \leftrightarrow |-\rangle$ transition is optically forbidden by angular momentum selection rules. In the far-detuned regime, the single-photon transitions are suppressed, and the system's dynamics is mediated by two-photon processes. They can be described in terms of an effective two-level model resembling the Kondo model. Using this effective description, we solve exactly the dynamics of the local system driven by a coherent pulse of an arbitrary elliptic polarization and compute observables of a scattered field,

including a polarization resolved inelastic power spectrum and second-order correlation functions.

We note that our model should be distinguished from the other quantum optical models studied in the literature which are somewhat related to the Kondo model. These models include a mapping of the strong coupling regime between a one-dimensional waveguide and a two-level system onto a bosonized form of the anisotropic Kondo model [53–56], a microwave realization of the ohmic spin-boson model [57,58], and the photon-assisted Kondo effect studied in Refs. [59,60].

II. MODEL

A. General considerations

Let us start our consideration from the three level Λ -scheme shown in Fig. 1. It is irradiated by a coherent light of an arbitrary elliptic polarization, i.e., a superposition of left- and right-polarized photons, and of a frequency ω_0 , which is half as big as the frequency ω_3 of the single-photon transitions $|+\rangle \leftrightarrow |3\rangle$ and $|-\rangle \leftrightarrow |3\rangle$.

While in this far-detuned regime single-photon processes are blocked by the energy conservation, the dominant processes will involve two photons. There are four possible second-order processes: (i) $|-\rangle \rightarrow |3\rangle \rightarrow |+\rangle$; (ii) $|+\rangle \rightarrow |3\rangle \rightarrow |-\rangle$; (iii) $|-\rangle \rightarrow |3\rangle \rightarrow |-\rangle$; and (iv) $|+\rangle \rightarrow |3\rangle \rightarrow |+\rangle$. The processes (i) and (ii) are shown in Fig. 1: One can recognize the inelastic Raman scattering, during which the scattered photon changes its energy (i) either by losing the amount $\hbar\Delta$ (Stokes scattering) or (ii) by gaining the amount $\hbar\Delta$ (anti-Stokes scattering). The parameter Δ is called the two-photon detuning. Both processes also change a polarization σ of an incoming photon. The processes (iii) and (iv) occur without energy and polarization changes, and they correspond to the Rayleigh scattering.

From this consideration, we conclude that the power spectrum of this model exhibits three peaks: one central peak at $\omega = \omega_0$ and two-side peaks at $\omega = \omega_0 \pm \Delta$. This qualitative analysis, however, misses lineshapes of these transitions, as well as the precise value (denoted by Ω in the following) of the Stokes and anti-Stokes shifts, which differs from Δ by field renormalization effects. In addition to the elastic Rayleigh

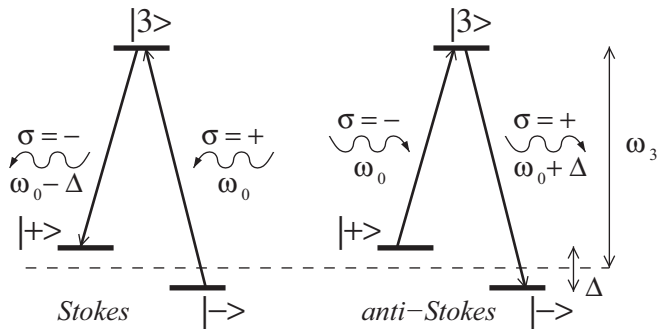


FIG. 1. Level structure of the local far-detuned Λ system. Direct transitions between the states $|+\rangle$ and $|-\rangle$ are forbidden by angular momentum selection rules. They are connected by second-order (Stokes and anti-Stokes) processes changing polarizations (σ) and frequency (ω_0) of incoming photons. Δ denotes the two-photon detuning, and we assume $\Delta \ll \omega_0 \approx \frac{\omega_3}{2}$.

peak, as we will show in the following, there is an inelastic, i.e., broadened, peak at $\omega = \omega_0$.

To quantitatively describe all these effects, we need an effective model describing the second-order transitions between the states $|+\rangle$ and $|-\rangle$, that is operating in terms of a two-level system. Its derivation will be a subject of the following subsection.

We note that interesting phenomena can arise only at $\Delta \neq 0$: For $\Delta = 0$ inelastic processes cannot take place, and therefore no entanglement between the local system and the scattered field is expected.

B. Derivation of the model

The Hamiltonian describing the three level system in Fig. 1 reads

$$H^{(3)} = \omega_3 |3\rangle\langle 3| + \Delta S_z + \sum_{\sigma=\pm} \int d\omega \omega a_{\omega\sigma}^\dagger a_{\omega\sigma} + \sum_{\sigma=\pm} \int d\omega g_\sigma [\sigma a_{\omega\sigma} |3\rangle\langle -\sigma| + \text{H.c.}], \quad (1)$$

where $S_z \equiv \frac{1}{2}(|+\rangle\langle +| - |-\rangle\langle -|)$, and $a_{\omega\sigma}^\dagger$ and $a_{\omega\sigma}$ are canonical bosonic creation and annihilation operators which create or destroy a photon with frequency ω and either right polarization ($\sigma = +$) or left polarization ($\sigma = -$). In our calculations, we set $\hbar = v = 1$, where v is the phase velocity of photons with a linear spectrum. The first line of Eq. (1) contains the free Hamiltonians of the local three-level system and of the waveguide radiation modes, while the second line contains the dipole interaction term in the rotating-wave approximation. The latter induces transitions $|-\rangle \leftrightarrow |3\rangle$ and $|+\rangle \leftrightarrow |3\rangle$ of the local system by means of absorption and emission of photons with right and left polarization, respectively. Matrix elements connecting the states $|-\rangle$ and $|+\rangle$ vanish identically in accordance with the angular momentum selection rules, as stated in the introduction.

When a driving field is far off resonance to the transitions $|-\rangle \leftrightarrow |3\rangle$ and $|+\rangle \leftrightarrow |3\rangle$, the state $|3\rangle$ becomes virtual; i.e., it can only be occupied during an infinitesimally short time. Then, the energy-conserving processes are of the second order in the coupling g , i.e., they involve two photons.

To make this explicit, we perform the (unitary) Schrieffer-Wolff transformation [61],

$$H^{(3)} \mapsto e^S H^{(3)} e^{-S} = H^{(3)} + [S, H^{(3)}] + \frac{1}{2}[S, [S, H^{(3)}]] + \dots, \quad (2)$$

which eliminates single-particle processes and gives rise to an effective—cotunneling—model. It is achieved by a choice of the generator

$$S = \sum_{\sigma=\pm} \int d\omega \Lambda_{\omega\sigma} [\sigma a_{\omega\sigma} |3\rangle\langle -\sigma| - \text{H.c.}] \quad (3)$$

with $\Lambda_{\omega\sigma} = \frac{g_\sigma}{\omega_3 - \omega} \approx \frac{2g_\sigma}{\omega_3}$ (assuming $\omega \approx \frac{\omega_3}{2}$). Truncating (2) after the double commutator and projecting the result onto the subspace of the local system spanned by the states $|+\rangle$ and $|-\rangle$, we obtain for $g_+ = g_- \equiv g$ (see Appendix A for details

of the derivation) an effective two-level Hamiltonian

$$H^{(2)} = \Delta S_z + \sum_{\sigma} \int d\omega \omega a_{\omega\sigma}^{\dagger} a_{\omega\sigma} + 2\pi J \left[\mathbf{s}(0) \cdot \mathbf{S} - \frac{n(0)}{4} \right], \quad (4)$$

where

$$J = \frac{4g^2}{\omega_3} > 0 \quad (5)$$

is the antiferromagnetic exchange coupling between the local spin- $\frac{1}{2}$

$$S^i = \sum_{\sigma, \sigma'} |\sigma\rangle \frac{\sigma_{\sigma\sigma'}^i}{2} \langle \sigma'| \quad (6)$$

and the reservoir spin density

$$s^i(0) = \sum_{\sigma, \sigma'} \int \frac{d\omega d\omega'}{2\pi} a_{\omega\sigma}^{\dagger} \frac{\sigma_{\sigma\sigma'}^i}{2} a_{\omega'\sigma'}. \quad (7)$$

Both S^i and $s^i(0)$ are expressed in terms of the Pauli matrices σ^i , $i = x, y, z$. Additionally, the reservoir particle density is defined by

$$n(0) = \sum_{\sigma} \int \frac{d\omega d\omega'}{2\pi} a_{\omega\sigma}^{\dagger} a_{\omega'\sigma}. \quad (8)$$

Apart from the difference in statistics of particles, the Hamiltonian (4) represents the (isotropic) Kondo model. It can be used for a description of the coherently driven Λ atom in the far-detuned regime in terms of a pseudo-spin- $\frac{1}{2}$ system which is antiferromagnetically coupled to the polarization density of a bosonic bath. Note that for $g_+ \neq g_-$ one obtains the anisotropic Kondo model with $J_{\parallel} = \frac{2(g_+^2 + g_-^2)}{\omega_3}$ and $J_{\perp} = \frac{4g_+g_-}{\omega_3}$, which, however, will not be studied in this paper.

Despite the similarity of the Hamiltonians, there are also essential differences between the electronic (fermionic) and the photonic (bosonic) Kondo models.

First of all, the fields in the two models obey different kinds of statistics. In the fermionic case, the Pauli exclusion principle restricts the set of possible states, while there is no such restriction in the bosonic case. Hence, the initial states that are considered in the two models are significantly different. In the electronic Kondo model, as an initial state one usually considers the Fermi sea (at zero temperature), while in the photonic case one often chooses a single-mode coherent state with a large mean number of photons in order to describe a laser field. Due to the properties of a coherent state one can obtain an *exact analytic solution* of the Heisenberg equations of motion in the photonic model, which is hardly possible in its electronic counterpart.

Second, observables and methods of their measurements are also different. In the electronic case, one typically measures a current through the sample (for more than one attached reservoir) and its autocorrelations and noise spectra. In the photonic case, one can measure both the average field and its correlation functions, which characterize the statistical properties of the electromagnetic field after interaction, as will be shown below.

For these reasons, we do not associate any kind of the *Kondo effect* to the photonic model, in the sense of how this effect is detected and interpreted in the electronic context (e.g., in a form of the quasiparticle—Kondo—resonance, being observed in the differential conductance in the zero bias limit and having a characteristic scale, called the Kondo temperature).

There are, however, some general features shared by the electronic Kondo and the photonic Kondo-like models: (i) one can still interpret virtual cotunneling processes in the same terms, as was discussed in Sec. II A; (ii) the two models basically describe the same kind of interaction, namely the exchange coupling of a local (pseudo-)spin- $\frac{1}{2}$ to a spin density of bath states, implying that in both cases scattering occurs due to spin fluctuations.

C. Time evolution of the local system

Using the effective two-level Hamiltonian (4) and the canonical commutation relations of the bosonic field operators, we find the Heisenberg equations of motion for the field operators

$$\frac{d}{dt} a_{\omega\sigma}(t) = -i\omega a_{\omega\sigma}(t) - iJ \sum_{\sigma'} \int d\omega' M_{\sigma\sigma'}(t) a_{\omega'\sigma'}(t), \quad (9)$$

where

$$M_{\sigma\sigma'}(t) = \frac{\sigma_{\sigma\sigma'}^i}{2} S^i(t) - \frac{\delta_{\sigma\sigma'}}{4}. \quad (10)$$

Assuming $t > x > 0$ we derive (see Appendix B for details) the relation

$$\begin{aligned} a_{\sigma}(x, t) &= \frac{1}{\sqrt{2\pi}} \int d\omega a_{\omega\sigma}(t) e^{i\omega x} \\ &= \sum_{\sigma'} \left[e^{i\phi} P_{\sigma\sigma'}^s(t-x) + P_{\sigma\sigma'}^t(t-x) \right] a_{\sigma'}(x-t, 0), \end{aligned} \quad (11)$$

where $a_{\sigma}(x, t)$ is the coordinate representation of the annihilation operator. The phase $\phi = 2 \arctan \pi J \approx 2\pi J$ separates the projectors

$$P_{\sigma\sigma'}^s(t) = -M_{\sigma\sigma'}(t), \quad (12)$$

$$P_{\sigma\sigma'}^t(t) = \delta_{\sigma\sigma'} + M_{\sigma\sigma'}(t), \quad (13)$$

onto the singlet (P^s) and the triplet (P^t) configurations, which are formed of the local spin and the itinerant spin density.

From Eqs. (4) and (11) we deduce the Heisenberg equation of motion for the local spin operators

$$\begin{aligned} \frac{d}{dt} S^i(t) &= 2\pi J \epsilon_{ijk} \sum_{\sigma, \sigma'} a_{\sigma}^{\dagger}(0, t) \frac{\sigma_{\sigma\sigma'}^j}{2} S^k(t) a_{\sigma'}(0, t) + \Delta \epsilon_{izk} S^k(t) \\ &= 2\pi J \cos^2 \frac{\phi}{2} \sum_{\sigma, \sigma'} a_{\sigma}^{\dagger}(-t, 0) \epsilon_{ijk} \frac{\sigma_{\sigma\sigma'}^j}{2} S^k(t) a_{\sigma'}(-t, 0) \\ &\quad + \frac{\pi J \sin \phi}{2} \sum_{\sigma, \sigma'} a_{\sigma}^{\dagger}(-t, 0) \left[\frac{\sigma_{\sigma\sigma'}^i}{2} - \delta_{\sigma\sigma'} S^i(t) \right] a_{\sigma'}(-t, 0) \\ &\quad + \Delta \epsilon_{izk} S^k(t). \end{aligned} \quad (14)$$

To analyze dynamics of the local system on the basis of Eq. (14), we need to explicitly define an initial state of the field.

D. Dynamics starting from the initial coherent state

We assume the field to be initially in a coherent state with frequency ω_0 and an arbitrary elliptic polarization. It is generated by the wave-packet operator, e.g., of a rectangular shape,

$$D|\text{vac}\rangle = \prod_{\sigma=\pm} D_{\sigma}|\text{vac}\rangle = \prod_{\sigma=\pm} \mathcal{N}_{\sigma} \exp\left[\frac{\alpha_{\sigma}}{\sqrt{L}} \int_{-L}^0 dx e^{i\omega_0 x} a_{\sigma}^{\dagger}(x)\right] |\text{vac}\rangle, \quad (15)$$

where $|\text{vac}\rangle$ denotes the photonic vacuum state, \mathcal{N}_{\pm} is a normalization constant, L is a spatial length of the rectangular pulse, and α_{\pm} are coherence parameters of the corresponding polarization.

In terms of the coherence parameters α_{\pm} , a polarization of the initial coherent state (15) is given by the classical Jones vector [62]

$$s_{cl} = \sum_{\sigma,\sigma'} \alpha_{\sigma}^* \frac{\sigma_{\sigma\sigma'}}{2L} \alpha_{\sigma'} = \frac{f}{2} \mathbf{n}_{cl}, \quad (16)$$

where \mathbf{n}_{cl} is a unit vector and $f = \sum_{\sigma} \frac{|\alpha_{\sigma}|^2}{L}$ is the photon density. In particular, the Jones vector parallel to $\pm \mathbf{e}_z$ corresponds to right- and left-circularly-polarized light, while the Jones vectors in the x - y plane correspond to linear polarizations (note that the point \mathbf{e}_x on the Jones sphere gives a polarization along \mathbf{e}_x in real space, while the point $-\mathbf{e}_x$ on the Jones sphere gives a polarization along \mathbf{e}_y in real space). Any other point on the Jones sphere corresponds to an elliptic polarization; opposite points parametrize mutually orthogonal polarizations.

In averaging Eq. (14) over the initial state (15) we use the property

$$a_{\sigma}(x,0) D_{\sigma} |\text{vac}\rangle = \Theta(-x) \Theta(x+L) \frac{\alpha_{\sigma}}{\sqrt{L}} e^{i\omega_0 x} D_{\sigma} |\text{vac}\rangle \quad (17)$$

and obtain the equation of motion governing dynamics of the spin expectation values at times $0 < t < L$ (i.e., as long as the spin is driven)

$$\frac{d}{dt} \langle \mathbf{S}(t) \rangle = \mathbf{h}_{\text{eff}} \times \langle \mathbf{S}(t) \rangle - \Gamma \left[\langle \mathbf{S}(t) \rangle - \frac{\mathbf{n}_{cl}}{2} \right], \quad (18)$$

where

$$\mathbf{h}_{\text{eff}} = \pi J f \cos^2 \frac{\phi}{2} \mathbf{n}_{cl} + \Delta \mathbf{e}_z \equiv \Omega_0 \mathbf{n}_{cl} + \Delta \mathbf{e}_z, \quad (19)$$

$$\Gamma = \frac{\pi}{2} J f \sin \phi. \quad (20)$$

The term $\Omega_0 \mathbf{n}_{cl}$ in the former equation represents the Lamb shift of the Zeeman field $\Delta \mathbf{e}_z$. At times $t > L$, when the driving is off, the spin will freely precess about the z axis with frequency Δ .

The solution of Eq. (18) reads

$$\begin{aligned} \langle \mathbf{S}(t) \rangle &= \langle \mathbf{S} \rangle_{st} + P_{n_h} [\langle \mathbf{S} \rangle_0 - \langle \mathbf{S} \rangle_{st}] e^{-\Gamma t} \\ &+ (1 - P_{n_h}) [\langle \mathbf{S} \rangle_0 - \langle \mathbf{S} \rangle_{st}] e^{-\Gamma t} \cos \Omega t \end{aligned}$$

$$+ \mathbf{n}_h \times [\langle \mathbf{S} \rangle_0 - \langle \mathbf{S} \rangle_{st}] e^{-\Gamma t} \sin \Omega t, \quad (21)$$

where we have introduced

$$\Omega = |\mathbf{h}_{\text{eff}}|, \quad \mathbf{n}_h = \frac{\mathbf{h}_{\text{eff}}}{\Omega}, \quad (22)$$

and P_{n_h} is a projector onto the unit vector \mathbf{n}_h .

As one can see from (18), the Bloch vector of the local spin precesses with the angular frequency Ω about the axis parallel to \mathbf{n}_h . All components of $\mathbf{S}(t)$, both longitudinal and transverse, decay with the same decay rate Γ . Both parameters Ω and Γ essentially depend on the photon density f and hence on the incoming power of the pulse. The precession axis \mathbf{n}_h has nontrivial dependence on various parameters only when \mathbf{n}_h is noncollinear with \mathbf{e}_z (i.e., for any polarization other than purely right or purely left).

The stationary value of the Bloch vector is given by

$$\langle \mathbf{S} \rangle_{st} = \frac{\mathbf{n}_{cl} + \lambda \mathbf{n}_h \times \mathbf{n}_{cl} + \lambda^2 \cos \psi \mathbf{n}_h}{2(1 + \lambda^2)}, \quad (23)$$

where $\lambda = \Omega/\Gamma$ and $\cos \psi = \mathbf{n}_h \cdot \mathbf{n}_{cl}$, while the initial expectation value $\langle \mathbf{S} \rangle_0 = \langle \mathbf{S}(t=0) \rangle$ is expressed via initial probability amplitudes of the states $|+\rangle$ and $|-\rangle$. We assume the absence of initial correlations between photons and the spin, which in particular means that the spin is initially in a pure state. This implies the normalization $|\langle \mathbf{S} \rangle_0| = \frac{1}{2}$.

The stationary regime (23) is reached at times $t \gg 1/\Gamma$. On the other hand, Eq. (18) holds for $t < L$. Therefore, the necessary condition for reaching the steady state is $\Gamma L \gg 1$, and it imposes a limitation on the drive amplitude $\sum_{\sigma} |\alpha_{\sigma}|^2 \gg 1/(\pi J)^2 \gg 1$, that is, the drive must be rather strong.

E. Purity and entanglement

During time evolution, the norm of the Bloch vector becomes smaller than $\frac{1}{2}$, which means that the spin reduced density matrix $\rho_s(t)$ corresponds to a mixed state. It is convenient to characterize the latter by the purity

$$\gamma(t) = \text{tr} \rho_s^2(t) = \frac{1 + 4 \langle \mathbf{S}(t) \rangle^2}{2}, \quad (24)$$

which in general takes values in the range between $\frac{1}{2}$ (maximally mixed state with the maximal entropy $\ln 2$) and 1 (pure state, zero entropy).

The purity (24) also serves as a measure of entanglement between the spin and the outgoing field. A state of the whole system can be generally written as $|\Psi\rangle = |+\rangle |\psi_a\rangle + |-\rangle |\psi_b\rangle$, where $|\psi_{a,b}\rangle$ are many-body states of the scattered field, which are not necessarily orthogonal to each other. It is always possible to choose orthonormal bases $|s_{\pm}\rangle$ and $|\chi_{a,b}\rangle$ for the spin and the field, respectively, in which $|\Psi\rangle = \sqrt{p_+} |s_+\rangle |\chi_a\rangle + \sqrt{p_-} |s_-\rangle |\chi_b\rangle$, $p_+ + p_- = 1$. The spin reduced density matrix $\rho_s = p_+ |s_+\rangle \langle s_+| + p_- |s_-\rangle \langle s_-|$ is characterized by the purity $\gamma = 1 - 2p_+ p_-$. Thus, the pure spin states, which occur when either $p_+ = 0$ or $p_- = 0$, correspond to the product states $|\Psi\rangle = |s_-\rangle |\chi_b\rangle$ and $|\Psi\rangle = |s_+\rangle |\chi_a\rangle$, while the spin state with the maximal entropy, which occurs at $p_+ = p_- = \frac{1}{2}$, corresponds to the maximally entangled state $|\Psi\rangle = \frac{1}{\sqrt{2}} (|s_+\rangle |\chi_a\rangle + |s_-\rangle |\chi_b\rangle)$. Alternatively, the purity can be expressed in terms of the field states $\gamma = 1 - 2(|\psi_a|^2 |\psi_b|^2 - |\langle \psi_a | \psi_b \rangle|^2)$.

In the stationary regime, we find

$$\gamma_{st} = \frac{1 + \frac{1}{4}\lambda^2(3 + \cos 2\psi)}{1 + \lambda^2}. \quad (25)$$

The pure state occurs for $\psi = 0$ and $\psi = \pi$. There are two cases when this state can be reached.

(1) If $\Delta = 0$, we find $\mathbf{n}_h = \mathbf{n}_{cl}$, and therefore $\psi = 0$. This case corresponds to a degenerate two-level system which obviously cannot change energies of incoming photons in the long time limit, and hence it cannot mediate inelastic processes, which might lead to an entanglement between the field and the spin. Thus, the steady state of these two subsystems is factorizable, and the purity approaches unity. This observation confirms our argument stated in Sec. II A.

(2) If either α_- or α_+ vanishes, we also find $\mathbf{n}_{cl} = \pm \mathbf{e}_z$ and $\mathbf{n}_h = \pm \mathbf{e}_z$, and thus $\psi = 0$ or $\psi = \pi$. This case corresponds to a right- or left-circularly polarized incident beam of photons. Suppose that we have the right-polarized beam (the Jones vector $s_{cl} = \frac{f}{2}\mathbf{e}_z$), which drives the transition $|-\rangle \leftrightarrow |3\rangle$. Since the state $|3\rangle$ can decay into both states $|+\rangle$ and $|-\rangle$, the local system eventually ends up in the state $|+\rangle$, corresponding to the Bloch vector $\frac{1}{2}\mathbf{e}_z$. This mechanism is analogous to STIRAP [26].

If neither of these conditions is met, that is, if the field is elliptically polarized and Δ is finite, the field and the local system will finally end up in an entangled state. The resulting field is not coherent anymore, and therefore the field-field correlation functions do not factorize. This is accompanied by inelastic scattering of photons into modes different from the input mode ω_0 .

The maximal degree of entanglement is achieved for $\psi \approx \frac{\pi}{2}$ and $\lambda \gg 1$, that is, for a linear polarization of the incoming

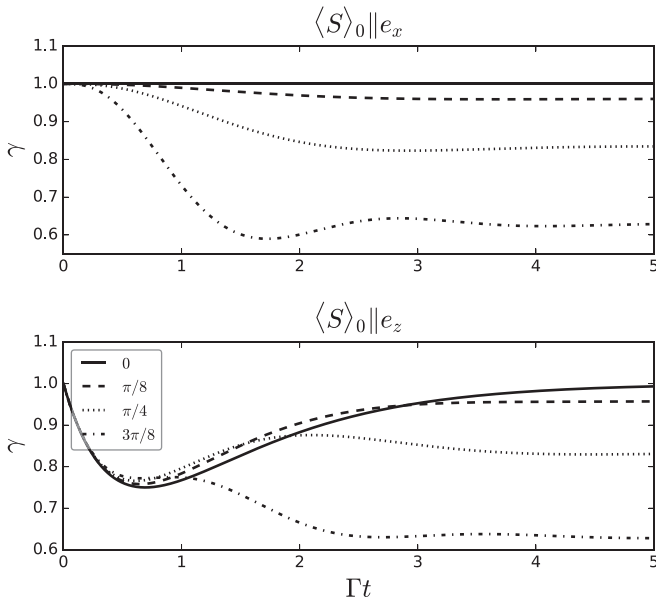


FIG. 2. Purity $\gamma(t)$ of the local two-level system for different values of $\psi = \arccos(\mathbf{n}_{cl} \cdot \mathbf{n}_h)$. For $\Delta \neq 0$, the stationary value of the purity is less than unity, while for $\Delta = 0$, the purity approaches unity (pure state) in the long time limit. Initial conditions are determined by the two different alignments, $\langle S \rangle_0 \parallel \mathbf{e}_x = \mathbf{n}_{cl}$ and $\langle S \rangle_0 \parallel \mathbf{e}_z \perp \mathbf{n}_{cl}$. Stationary values of the purity do not depend on an initial state.

field and a large two-photon detuning Δ . In this case, the processes with polarization flips are inefficient, and the field states $|\psi_a\rangle$ and $|\psi_b\rangle$ will predominantly consist of photons with left and right polarizations, respectively. For this reason, they are approximately orthogonal to each other. The mean numbers of left- and right-polarized photons are initially the same, and they will remain unchanged during interaction. This determines the equal weights of the states $|\psi_a\rangle$ and $|\psi_b\rangle$ in the state $|\Psi\rangle$ of the whole system and leads to the maximally entangled state.

In Fig. 2, we show time dependence of the purity for different alignments (parallel and perpendicular) of the initial Jones vector and the initial Bloch vector at various values of the two-photon detuning Δ . It also illustrates how the entanglement between the spin and the field is built up in time.

Having understood time dynamics of the local spin and its stationary values, we go over to a description of the field properties in the stationary limit.

III. FIRST-ORDER CORRELATION FUNCTIONS AND POWER SPECTRUM

Power spectra of three-level atoms were discussed in several papers over the years; see Refs. [34–42]. However, none of these studies has dealt with polarization effects in the excitation spectrum. Here, we fill up this gap by making exact calculations of the polarization-dependent power spectrum.

A. Polarization unresolved power spectrum

Using Eqs. (11) and (23), we can express the stationary value of the polarization unresolved field-field correlation function by

$$\begin{aligned} C^0(\tau) &= \sum_{\sigma} \langle a_{\sigma}^{\dagger}(x, t + \tau) a_{\sigma}(x, t) \rangle \\ &= f e^{i\omega_0\tau} \left[1 - \left(\frac{5}{4} - \gamma_{st} \right) \sin^2 \frac{\phi}{2} \right. \\ &\quad + \langle \mathbf{S}(t - x + \tau) \cdot \mathbf{S}(t - x) \rangle \sin^2 \frac{\phi}{2} \\ &\quad \left. + i \mathbf{n}_{cl} \cdot \langle \mathbf{S}(t - x + \tau) \times \mathbf{S}(t - x) \rangle \sin^2 \frac{\phi}{2} \right]. \quad (26) \end{aligned}$$

In this derivation, we also used the identity

$$[a_{\sigma}(-t - \tau, 0), S^i(t)] = 0 \quad \text{for } \tau > 0, \quad (27)$$

which follows from the commutation of the Heisenberg operators $[a_{\omega\sigma}(t), S^i(t)] = 0$ (see Appendix C for the proof). The relation (27) is a formal expression of the causality principle, stating that the free field at the position $x = -\tau < 0$ and time t (that is, to the left from the scatterer, and hence before interacting with it), which is described by the Schrödinger operator $a_{\sigma}(-t - \tau, 0)$, remains independent of the scatterer's state $S^i(t)$.

We can decompose (26) into elastic (or coherent) and inelastic (or incoherent) contributions

$$C^0(\tau) = C_{el}^0(\tau) + C_{inel}^0(\tau), \quad (28)$$

$$C_{el}^0(\tau) = f e^{i\omega_0\tau} \left[1 - \frac{3}{2}(1 - \gamma_{st}) \sin^2 \frac{\phi}{2} \right], \quad (29)$$

$$C_{\text{inel}}^0(\tau) = f e^{i\omega_0\tau} \sin^2 \frac{\phi}{2} \left[\langle \mathbf{S}(t+\tau) \cdot \mathbf{S}(t) \rangle - \langle \mathbf{S} \rangle_{st}^2 \right. \\ \left. + i \mathbf{n}_{cl} \cdot \langle \mathbf{S}(t+\tau) \times \mathbf{S}(t) \rangle \right]. \quad (30)$$

For $\tau > 0$, the equation of motion for $C^{ij}(\tau)$ in the long time limit reads

$$\frac{d}{d\tau} C^{ij}(\tau) = \Omega \epsilon_{ilk} n_h^l C^{kj}(\tau) - \Gamma \left[C^{ij}(\tau) - \frac{n_{cl}^i \langle S^j \rangle_{st}}{2} \right]. \quad (31)$$

Solving these equations we can compute (26) for $\tau \geq 0$. The Fourier transform of (26) with respect to τ yields the sought power spectrum. Providing the details of this calculation in Appendix C, we present the polarization unresolved power spectrum

$$\tilde{C}^0(\nu) = \frac{2\pi f}{\Omega} \delta(\nu) \left[1 - \frac{3}{2}(1 - \gamma_{st}) \sin^2 \frac{\phi}{2} \right] \\ + \frac{f(1 - \gamma_{st})}{\Gamma} \sin^2 \frac{\phi}{2} \left[\frac{1 + \nu \cos \psi}{1 + \lambda^2 \nu^2} \right. \\ \left. + \frac{1 - (\nu - 1) \cos^2 \frac{\psi}{2}}{1 + \lambda^2 (\nu - 1)^2} + \frac{1 + (\nu + 1) \sin^2 \frac{\psi}{2}}{1 + \lambda^2 (\nu + 1)^2} \right], \quad (32)$$

where $\nu = (\omega - \omega_0)/\Omega$. Note that the inelastic power spectrum is proportional to $(1 - \gamma_{st})$, and it vanishes for the pure stationary state of the local system.

Figure 3 shows $\tilde{C}_{\text{inel}}^0(\nu)$ for various values of λ and ψ . It exhibits the three-peak structure, as suggested by the heuristic arguments made in Sec. II A. The resonances become sharper for increasing λ , which is achieved at a weak coupling J and a weak field f compared against Δ . The Stokes shift $\Omega = |\mathbf{h}_{\text{eff}}|$, given by the magnitude of an effective magnetic field experienced by the local system, can be extracted from this plot along with the peaks' broadenings Γ .

The shape of $\tilde{C}_{\text{inel}}^0(\nu)$ is invariant under simultaneous transformations $\nu \rightarrow -\nu$ and $\psi \rightarrow \psi + \frac{\pi}{2}$, which correspond to a sign change of Δ and an exchange of roles between the left and the right polarizations. Under the transformation $\nu \rightarrow -\nu$ alone, the power spectrum $\tilde{C}_{\text{inel}}^0(\nu)$ is not invariant, which means that the rates of the processes (i) and (ii) defined in Sec. II A are in general different and dependent on the initial polarization of the field.

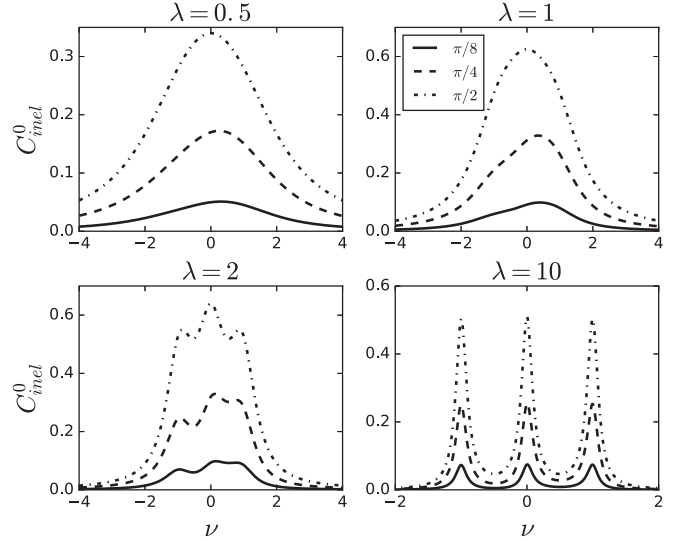


FIG. 3. Inelastic peaks in the polarization unresolved power spectra, Eq. (32). The legend in the upper right panel indicates the values of ψ , which apply to all panels. For large values of $\Delta \gg Jf$ (which implies $\lambda \gg 1$), the peaks are well resolved, and one can extract the values of Ω and Γ .

The integrated output power amounts to

$$P_{\text{tot}} = \frac{\Omega}{2\pi} \int d\nu (\nu\Omega + \omega_0) \tilde{C}^0(\nu) = \omega_0 f, \quad (33)$$

and thereby it is conserved. The inelastic contribution to it is given by

$$P_{\text{inel}} = \frac{3\omega_0 f}{2} (1 - \gamma_{st}) \sin^2 \frac{\phi}{2}. \quad (34)$$

B. Polarization resolved spectral function

To probe cross-correlations between different polarizations, it is useful to define the polarization resolved first-order correlation function

$$C^d(\tau) = \sum_{\sigma, \sigma'} \langle a_{\sigma}^{\dagger}(x, t + \tau) \frac{\delta_{\sigma\sigma'} + n_d^i \sigma_{\sigma'}^i}{2} a_{\sigma'}(x, t) \rangle \\ = C^0(\tau) + \mathbf{n}_d \cdot \mathbf{C}_s(\tau), \quad (35)$$

which resolves photonic polarizations parallel to $\pm \mathbf{n}_d$. The unit vector \mathbf{n}_d thus defines a detector's polarization.

Using Eq. (11), we express $\mathbf{C}_s(\tau)$ in the long time limit as a sum of elastic and inelastic contributions

$$\mathbf{C}_s(\tau) = \mathbf{C}_{s,\text{el}}(\tau) + \mathbf{C}_{s,\text{inel}}(\tau), \quad (36)$$

$$\mathbf{C}_{s,\text{el}}(\tau) = \frac{f}{2} e^{i\omega_0\tau} \left[\cos^2 \frac{\phi}{2} \mathbf{n}_{cl} + 2 \sin^2 \frac{\phi}{2} \langle \mathbf{S} \rangle_{st} - \sin \phi \mathbf{n}_{cl} \times \langle \mathbf{S} \rangle_{st} \right] + \frac{f}{4} e^{i\omega_0\tau} \sin^2 \frac{\phi}{2} (1 - \gamma_{st}) (\mathbf{n}_{cl} - 4 \langle \mathbf{S} \rangle_{st}), \quad (37)$$

$$\mathbf{C}_{s,\text{inel}}(\tau) = \frac{f}{2} e^{i\omega_0\tau} \sin^2 \frac{\phi}{2} \left[\langle \mathbf{S}(t+\tau) (\mathbf{n}_{cl} \cdot \mathbf{S}(t)) \rangle + \langle (\mathbf{n}_{cl} \cdot \mathbf{S}(t+\tau)) \mathbf{S}(t) \rangle - 2 (\mathbf{n}_{cl} \cdot \langle \mathbf{S} \rangle_{st}) \langle \mathbf{S} \rangle_{st} \right. \\ \left. - \mathbf{n}_{cl} (\langle \mathbf{S}(t+\tau) \cdot \mathbf{S}(t) \rangle - \langle \mathbf{S} \rangle_{st}^2) - i \langle \mathbf{S}(t+\tau) \times \mathbf{S}(t) \rangle \right], \quad (38)$$

where the inelastic contribution is expressed via the spin-spin correlation functions.

From Eq. (B6), we get at $t, x \gg 1/\Gamma$ the stationary value of the average field

$$\langle a_{\sigma}(x, t) \rangle_{st} = \frac{e^{i\omega_0(x-t)}}{\sqrt{L}} \sum_{\sigma'} U_{\sigma\sigma'} \alpha_{\sigma'},$$

$$U_{\sigma\sigma'} = \frac{1 - e^{i\phi}}{2} \sigma_{\sigma\sigma'}^i S_{st}^i + \frac{3 + e^{i\phi}}{4} \delta_{\sigma\sigma'}. \quad (39)$$

Its polarization is parameterized by the new Jones vector

$$\mathbf{s}_q \equiv \sum_{\sigma, \sigma'} \langle a_{\sigma}^{\dagger}(x, t) \rangle_{st} \frac{\boldsymbol{\sigma}_{\sigma\sigma'}}{2} \langle a_{\sigma'}(x, t) \rangle_{st} = \mathbf{C}_{s, \text{el}}(0). \quad (40)$$

We label it by the subscript q to indicate that the initially classical state is affected by interaction with the quantum system. In the absence of interaction ($\phi = 0$) we recover $\mathbf{s}_q = \mathbf{s}_{cl}$.

In Fig. 4 we plot the angle θ parameterizing a degree of ellipticity in a polarization of the emitted radiation, provided that initially it was linear, $\mathbf{n}_{cl} = \mathbf{e}_x$. Although a type of polarization changes very slightly from the incoming to the outgoing pulse, one can experimentally extract the quantity $\frac{\Delta}{\pi J \cos^2 \frac{\phi}{2}}$ by measuring a polarization of the average emitted field at various powers of the incoming signal $\propto f$ and fitting the result to the curves in Fig. 4. In other words, by polarization measurements one can find the ratio Ω_0/Δ for given f . Combining this result with the ratio Ω/Γ extracted from the power spectra shown in Fig. 3, it becomes possible to find the values of Δ/Γ and Ω_0/Γ , characterizing the local system.

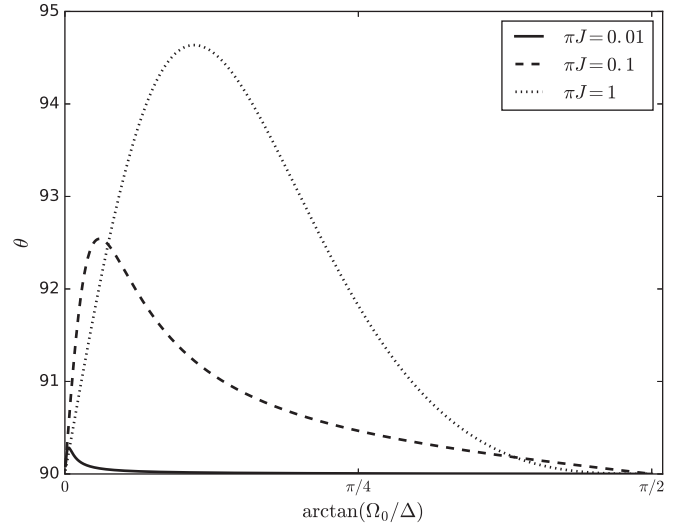


FIG. 4. Ellipticity $\theta = \arccos \frac{\mathbf{e}_z \cdot \mathbf{s}_q}{|\mathbf{s}_q|}$ (in degrees) as a function of the ratio between the two-photon detuning and its Lamb shift at various exchange couplings J . An initially linearly polarized light with $\mathbf{n}_{cl} = \mathbf{e}_x$ does not considerably change its type of polarization: Deviations from the equator on the Jones sphere do not exceed 5 deg.

Analogously to the unresolved case we compute the spin-spin correlators in Eq. (38) (see Appendix D for details). Performing the Fourier transform of (D31), we find the direction-dependent part of the polarization resolved inelastic power spectrum

$$\begin{aligned} \tilde{\mathbf{C}}_{s, \text{inel}}(\nu) = & \frac{f}{2\Omega} \sin^2 \frac{\phi}{2} (1 - \gamma_{st}) \left\{ -\frac{\lambda \mathbf{n}_{cl} - 2\lambda \cos \psi \mathbf{n}_h + \mathbf{n}_{cl} \times \mathbf{n}_h}{\lambda^2 \nu^2 + 1} + \frac{\lambda \nu \mathbf{n}_h}{\lambda^2 \nu^2 + 1} \right. \\ & + \frac{2\lambda \mathbf{n}_{cl} + 2\lambda(1 + \lambda^2 - \cos \psi) \mathbf{n}_h + (1 - \lambda^2) \mathbf{n}_{cl} \times \mathbf{n}_h}{2(1 + \lambda^2)[\lambda^2(\nu - 1)^2 + 1]} \\ & - \lambda(\nu - 1) \frac{(1 - \lambda^2) \mathbf{n}_{cl} + (1 + \lambda^2 + 2\lambda^2 \cos \psi) \mathbf{n}_h - 2\lambda \mathbf{n}_{cl} \times \mathbf{n}_h}{2(1 + \lambda^2)[\lambda^2(\nu - 1)^2 + 1]} \\ & + \frac{2\lambda \mathbf{n}_{cl} - 2\lambda(1 + \lambda^2 + \cos \psi) \mathbf{n}_h + (1 - \lambda^2) \mathbf{n}_{cl} \times \mathbf{n}_h}{2(1 + \lambda^2)[\lambda^2(\nu + 1)^2 + 1]} \\ & \left. + \lambda(\nu + 1) \frac{(1 - \lambda^2) \mathbf{n}_{cl} - (1 + \lambda^2 - 2\lambda^2 \cos \psi) \mathbf{n}_h - 2\lambda \mathbf{n}_{cl} \times \mathbf{n}_h}{2(1 + \lambda^2)[\lambda^2(\nu + 1)^2 + 1]} \right\}. \quad (41) \end{aligned}$$

In Fig. 5, we plot $g_{\mathbf{n}_d}^{(1)}(\nu) = \tilde{\mathbf{C}}^0(\nu) + \mathbf{n}_d \cdot \tilde{\mathbf{C}}_{s, \text{inel}}(\nu)$. In an experiment, we propose to use a detector which selects photons with a polarization parameterized by the unit vector \mathbf{n}_d . The polarization resolved inelastic power spectrum $g_{\mathbf{n}_d}^{(1)}(\nu)$ contains information about the weights of frequency modes to which these photons scatter. For the initial linear polarization along \mathbf{e}_x , we choose $\mathbf{n}_d = \pm \mathbf{e}_x$ (upper panel) and $\mathbf{n}_d = \pm \mathbf{e}_z$ (lower panels). The last two cases show the mean number of photons with right and left circular polarizations in different frequency modes which are produced by the local system from the linearly polarized input pulse.

We note that the effect of the polarization change is much more pronounced and detailed in the function $g_{\mathbf{n}_d}^{(1)}(\nu)$ than in

the polarization of the average field depicted in Fig. 4. In addition, we emphasize that the effective magnetic field \mathbf{h}_{eff} produced by the local system breaks the symmetry between the right- and left-circularly-polarized photons, since the vector \mathbf{n}_h necessarily lies in the x - z plane.

IV. SECOND-ORDER CORRELATION FUNCTION

Statistical properties of the emitted light are characterized by the second-order correlation functions

$$G_{\sigma_1' \sigma_2', \sigma_1 \sigma_2}^{(2)} = \langle a_{\sigma_1'}^{\dagger}(x, t) a_{\sigma_2'}^{\dagger}(x, t + \tau) a_{\sigma_2}(x, t + \tau) a_{\sigma_1}(x, t) \rangle. \quad (42)$$

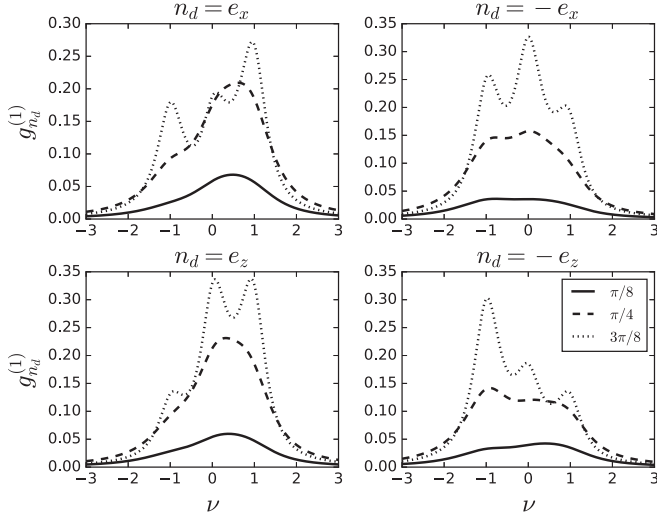


FIG. 5. Polarization resolved inelastic power spectrum for various values of ψ (shown in the legend) and detector polarizations \mathbf{n}_d . In particular, the two lower panels show how many photons with right and left circular polarizations can be produced from the initial pulse linearly polarized along \mathbf{e}_x .

It is more convenient to introduce the combinations

$$G_{n,m}(\tau) = \frac{1}{4} \sum_{\sigma'_2, \sigma_2} \sum_{\sigma'_1, \sigma_1} (\mathbf{n} \cdot \boldsymbol{\sigma}_{\sigma'_2 \sigma_2}) (\mathbf{m} \cdot \boldsymbol{\sigma}_{\sigma'_1 \sigma_1}) G_{\sigma'_1 \sigma'_2, \sigma_1 \sigma_2}^{(2)}, \quad (43)$$

$$G_{n,0}(\tau) = \frac{1}{2} \sum_{\sigma'_2, \sigma_2} \sum_{\sigma_1} (\mathbf{n} \cdot \boldsymbol{\sigma}_{\sigma'_2 \sigma_2}) G_{\sigma_1 \sigma'_2, \sigma_1 \sigma_2}^{(2)}, \quad (44)$$

$$G_{0,m}(\tau) = \frac{1}{2} \sum_{\sigma_2} \sum_{\sigma'_1, \sigma_1} (\mathbf{m} \cdot \boldsymbol{\sigma}_{\sigma'_1 \sigma_1}) G_{\sigma'_1 \sigma_2, \sigma_1 \sigma_2}^{(2)}, \quad (45)$$

$$G_{0,0}(\tau) = \sum_{\sigma_2} \sum_{\sigma_1} G_{\sigma_1 \sigma_2, \sigma_1 \sigma_2}^{(2)}, \quad (46)$$

and consequently

$$\begin{aligned} g_{n,m}^{(2)}(\tau) &= \left[G_{n,m}(\tau) + \frac{G_{0,m}(\tau) + G_{n,0}(\tau)}{2} + \frac{G_{0,0}(\tau)}{4} \right] \\ &\times \left[G_{n,m}(\infty) + \frac{G_{0,m}(\infty) + G_{n,0}(\infty)}{2} + \frac{G_{0,0}(\infty)}{4} \right]^{-1}. \end{aligned} \quad (47)$$

Physical meaning of the latter function is transparent: The second (first) index indicates the polarization vector of the first (second) measured photon in coincidence measurements with delay time τ .

To find the quantities (43)–(46) we use the relations directly following from (11):

$$\begin{aligned} \sum_{\sigma', \sigma} a_{\sigma'}^\dagger(x, t) \frac{\boldsymbol{\sigma}_{\sigma' \sigma}}{2} a_{\sigma}(x, t) &= \sum_{\sigma', \sigma} a_{\sigma'}^\dagger(x - t, 0) \frac{1}{2} \left[\cos^2 \frac{\phi}{2} \boldsymbol{\sigma}_{\sigma' \sigma} + \sin^2 \frac{\phi}{2} \delta_{\sigma' \sigma} \mathbf{S}(t - x) \right. \\ &\left. - \sin \phi \boldsymbol{\sigma}_{\sigma' \sigma} \times \mathbf{S}(t - x) \right] a_{\sigma}(x - t, 0), \end{aligned} \quad (48)$$

$$\sum_{\sigma} a_{\sigma}^\dagger(x, t) a_{\sigma}(x, t) = \sum_{\sigma} a_{\sigma}^\dagger(x - t, 0) a_{\sigma}(x - t, 0). \quad (49)$$

They allow us to find (see Appendix E for details) that in the stationary limit

$$G_{n,m}(\tau) = \frac{f}{2} (\mathbf{m} \cdot \mathbf{C}_s(0)) \mathbf{n} \cdot \left[\cos^2 \frac{\phi}{2} \mathbf{n}_{cl} + 2 \sin^2 \frac{\phi}{2} \mathbf{k}_m(\tau) - \sin \phi \mathbf{n}_{cl} \times \mathbf{k}_m(\tau) \right], \quad (50)$$

$$G_{n,0}(\tau) = \frac{f^2}{2} \mathbf{n} \cdot \left[\cos^2 \frac{\phi}{2} \mathbf{n}_{cl} + 2 \sin^2 \frac{\phi}{2} \mathbf{k}_0(\tau) - \sin \phi \mathbf{n}_{cl} \times \mathbf{k}_0(\tau) \right], \quad (51)$$

$$G_{0,m}(\tau) = f (\mathbf{m} \cdot \mathbf{C}_s(0)), \quad (52)$$

$$G_{0,0}(\tau) = f^2, \quad (53)$$

where

$$\mathbf{C}_s(0) = \frac{f}{2} \left[\cos^2 \frac{\phi}{2} \mathbf{n}_{cl} + 2 \sin^2 \frac{\phi}{2} \langle \mathbf{S} \rangle_{st} - \sin \phi \mathbf{n}_{cl} \times \langle \mathbf{S} \rangle_{st} \right], \quad (54)$$

and the vectors $\mathbf{k}_0(\tau)$ and $\mathbf{k}_m(\tau)$

$$\frac{d}{d\tau} \mathbf{k}_0(\tau) = \Omega \mathbf{n}_h \times \mathbf{k}_0(\tau) - \Gamma \left[\mathbf{k}_0(\tau) - \frac{1}{2} \mathbf{n}_{cl} \right], \quad (55)$$

$$\frac{d}{d\tau} \mathbf{k}_m(\tau) = \Omega \mathbf{n}_h \times \mathbf{k}_m(\tau) - \Gamma \left[\mathbf{k}_m(\tau) - \frac{1}{2} \mathbf{n}_{cl} \right], \quad (56)$$

with initial condition given by

$$\mathbf{k}_0(0) = \langle \mathbf{S} \rangle_{st} \cos^2 \frac{\phi}{2} + \frac{1}{2} \mathbf{n}_{cl} \sin^2 \frac{\phi}{2} + \frac{1}{2} \mathbf{n}_{cl} \times \langle \mathbf{S} \rangle_{st} \sin \phi, \quad (57)$$

$$\begin{aligned} \mathbf{k}_m(0) &= \frac{f}{2(\mathbf{C}_s(0) \cdot \mathbf{m})} \left[(\mathbf{n}_{cl} \cdot \mathbf{m}) \langle \mathbf{S} \rangle_{st} \cos^2 \frac{\phi}{2} + \mathbf{n}_{cl} (\langle \mathbf{S} \rangle_{st} \cdot \mathbf{m}) \right. \\ &\left. \times \sin^2 \frac{\phi}{2} - \frac{\sin \phi}{4} \mathbf{m} \times (\mathbf{n}_{cl} - 2 \langle \mathbf{S} \rangle_{st}) \right]. \end{aligned} \quad (58)$$

It is remarkable that the major ingredients $\mathbf{k}_0(\tau)$ and $\mathbf{k}_m(\tau)$ of the second-order correlation function obey the same equations as the local spin [compare Eqs. (55) and (56) to Eq. (18)]. On the other hand, none of the equations for the first-order correlation function (either polarization unresolved or resolved) resembles the equation for the local spin. At first glance, this might seem to be a violation of the *quantum regression theorem* (see, e.g., Ref. [63] for its formulation). However, a deeper analysis shows that in the standard formulation of this theorem, the linearity of light-matter interaction in the field operators is required. In our case, this interaction is bilinear in fields, and therefore it becomes necessary to promote the quantum regression theorem to the

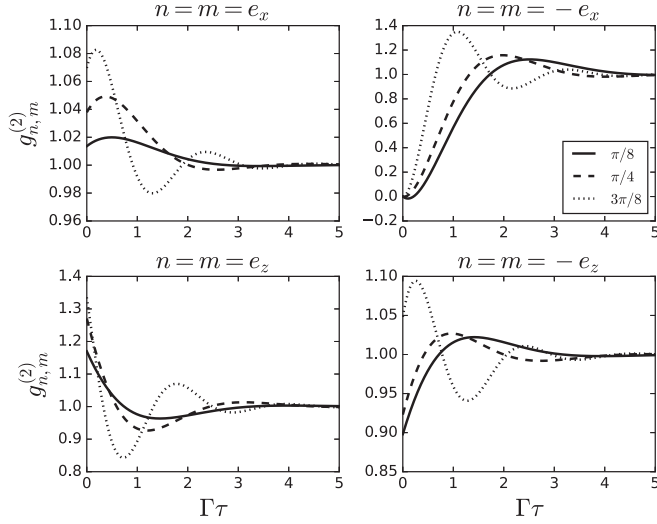


FIG. 6. Second-order correlation function $g_{n,m}^{(2)}(\tau)$ for various values of ψ (in the legend). The unit vectors \mathbf{n} and \mathbf{m} define polarizations of the detectors used in coincidence measurements and are aligned parallel to each other. The input signal is linearly polarized, $\mathbf{n}_{cl} = \mathbf{e}_x$.

level of second-order correlation functions, which we indeed see in the form of Eqs. (55) and (56).

It is now straightforward to find solutions of these equations. Analogously to Eq. (21) they read

$$\begin{aligned} \mathbf{k}(\tau) = & \langle \mathbf{S} \rangle_{st} + P_{n_h} [\mathbf{k}(0) - \langle \mathbf{S} \rangle_{st}] e^{-\Gamma\tau} \\ & + (1 - P_{n_h}) [\mathbf{k}(0) - \langle \mathbf{S} \rangle_{st}] e^{-\Gamma\tau} \cos \Omega\tau \\ & + \mathbf{n}_h \times [\mathbf{k}(0) - \langle \mathbf{S} \rangle_{st}] e^{-\Gamma\tau} \sin \Omega\tau, \end{aligned} \quad (59)$$

where \mathbf{k} is either \mathbf{k}_0 or \mathbf{k}_m .

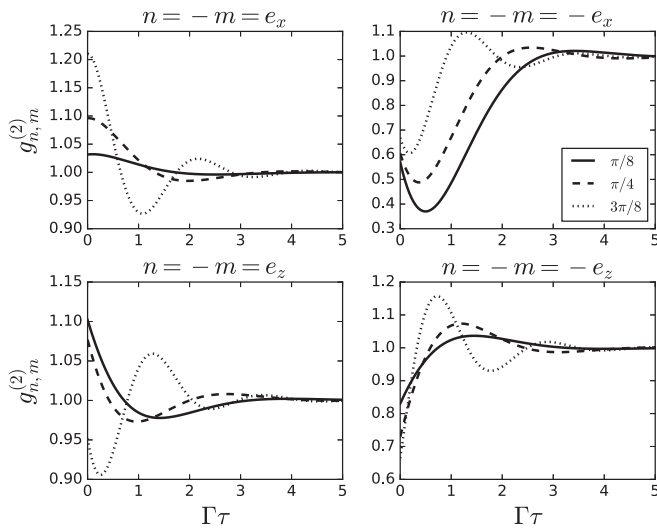


FIG. 7. Second-order correlation function $g_{n,m}^{(2)}(\tau)$ for various values of ψ (in the legend). The unit vectors \mathbf{n} and \mathbf{m} define polarizations of the detectors used in coincidence measurements and are aligned antiparallel to each other. The input signal is linearly polarized, $\mathbf{n}_{cl} = \mathbf{e}_x$.

Finally, we obtain

$$\begin{aligned} g_{n,m}^{(2)}(\tau) = & 1 + f \sin \frac{\phi}{2} \left[(\mathbf{m} \cdot \mathbf{C}_s(0)) (\mathbf{n} \cdot \mathbf{l}_m(\tau)) + \frac{f}{2} (\mathbf{n} \cdot \mathbf{l}_0(\tau)) \right] \\ & \times \left[\frac{f}{2} + \mathbf{m} \cdot \mathbf{C}_s(0) \right]^{-1} \left[\frac{f}{2} + \mathbf{n} \cdot \mathbf{C}_s(0) \right]^{-1}, \end{aligned} \quad (60)$$

where

$$\mathbf{l}(\tau) = \sin \frac{\phi}{2} [\mathbf{k}(\tau) - \langle \mathbf{S} \rangle_{st}] - \cos \frac{\phi}{2} \mathbf{n}_{cl} \times [\mathbf{k}(\tau) - \langle \mathbf{S} \rangle_{st}]. \quad (61)$$

In Figs. 6 and 7 we plot the function $g_{n,m}^{(2)}(\tau)$ for parallel and antiparallel alignments of the vectors \mathbf{n} and \mathbf{m} , defining detectors' polarizations. We see that emitted photons, either with linear or with circular polarizations, demonstrate diverse statistical features ranging from bunching to antibunching depending on the model parameters.

V. CONCLUSION

We derived the photonic analog of the Kondo model in the far-detuned regime of a three-level emitter coupled to waveguide modes with a linear dispersion and transitions between levels obeying angular momentum selection rules. The derived effective Hamiltonian coincides—except for statistics of particles—with the antiferromagnetic Kondo Hamiltonian arising in condensed-matter models.

Using the derived effective model we studied dynamics of the local system as well as various correlation functions of scattered light assuming the initially coherent state. It turned out that in the photonic Kondo-like model all inelastic properties are tightly bound to a driving field polarization. In addition, they also quantify the degree of entanglement between the local system and the outgoing radiation. We proposed a way of experimentally establishing the model parameters by performing various polarization-resolved measurements. We studied the statistical properties of the outgoing radiation and observed that they are sensitive to both model parameters and the initial polarization of the field. Moreover, the second-order coherence shows oscillatory behavior and can possibly be used to engineer strongly correlated states of light.

We also observed that the quantum regression theorem holds in our model for the second-order coherence connecting its dynamics to that of the local system. This is a consequence of the bilinear (in fields) light-matter coupling in the effective model. This feature is in contrast to standard applications of the quantum regression theorem to models with a linear coupling, where it relates local dynamics to the first-order coherence.

ACKNOWLEDGMENTS

The authors thank H. Schoeller and D. Schuricht for useful discussions. The work of V.G. is part of the Delta-ITP consortium, a program of the Netherlands Organization for Scientific Research (NWO) funded by the Dutch Ministry of Education, Culture and Science (OCW).

APPENDIX A: DERIVATION OF THE EFFECTIVE HAMILTONIAN (4) BY THE SCHRIEFFER-WOLFF TRANSFORMATION

The Schrieffer-Wolff transformation maps the three-level Hamiltonian (1) onto the effective two-level Hamiltonian

$$H^{(3)} \mapsto H^{(2)} = P e^S H^{(3)} e^{-S} P \approx P \{ H^{(3)} + [S, H^{(3)}] + \frac{1}{2} [S, [S, H^{(3)}]] \} P, \quad (\text{A1})$$

where the generator S is chosen in the form (3), and $P \equiv |+\rangle \langle +| + |-\rangle \langle -|$ is a projector onto the subspace spanned by the states $|+\rangle$ and $|-\rangle$.

Neglecting Δ against ω_3 we find

$$\begin{aligned} [S, H^{(3)}] &= \sum_{\sigma=\pm} \sigma \int d\omega \Lambda_{\omega\sigma} (\omega - \omega_3) (a_{\omega\sigma} |3\rangle \langle -\sigma| + a_{\omega\sigma}^\dagger |-\sigma\rangle \langle 3|) \\ &\quad - \sum_{\sigma, \sigma'=\pm} \sigma \sigma' \int d\omega d\omega' (g_\sigma \Lambda_{\omega'\sigma'} + g_{\sigma'} \Lambda_{\omega\sigma}) a_{\omega'\sigma'}^\dagger a_{\omega\sigma} |-\sigma'\rangle \langle -\sigma| \\ &\quad + \sum_{\sigma=\pm} \int d\omega d\omega' g_\sigma (\Lambda_{\omega'\sigma} + \Lambda_{\omega\sigma}) a_{\omega\sigma} a_{\omega'\sigma}^\dagger |3\rangle \langle 3| \end{aligned} \quad (\text{A2})$$

and

$$P[S, [S, H^{(3)}]]P = -2 \sum_{\sigma, \sigma'} \sigma \sigma' \int d\omega d\omega' \Lambda_{\omega'\sigma'} \Lambda_{\omega\sigma} \left(\frac{\omega' + \omega}{2} - \omega_3 \right) a_{\omega'\sigma'}^\dagger a_{\omega\sigma} |-\sigma'\rangle \langle -\sigma|. \quad (\text{A3})$$

Choosing $\Lambda_{\omega\sigma} = \frac{g_\sigma}{\omega_3 - \omega}$ to suppress in (A1) the terms linear in $a_{\omega\sigma}$ and $a_{\omega\sigma}^\dagger$, we arrive at the effective two-level Hamiltonian $H^{(2)}$

$$H^{(2)} = \Delta S_z + \sum_{\sigma} \int d\omega \omega a_{\omega\sigma}^\dagger a_{\omega\sigma} - \frac{1}{2} \sum_{\sigma, \sigma'} \sigma \sigma' \int d\omega d\omega' J_{\omega'\sigma', \omega\sigma} a_{\omega'\sigma'}^\dagger a_{\omega\sigma} |-\sigma'\rangle \langle -\sigma|, \quad (\text{A4})$$

where $J_{\omega'\sigma', \omega\sigma} = g_{\sigma'} g_\sigma \left(\frac{1}{\omega_3 - \omega'} + \frac{1}{\omega_3 - \omega} \right)$. This Hamiltonian can easily be transformed to the form (4) under additional assumptions $g_+ = g_- \equiv g$ and $J_{\omega'\sigma', \omega\sigma} = J_{\omega'\omega} \approx J_{\omega_3/2, \omega_3/2} = \frac{4g^2}{\omega_3} \equiv J$.

APPENDIX B: SOLVING EQUATIONS OF MOTION

Formally integrating (9) we obtain

$$\begin{aligned} a_{\omega\sigma}(t) &= e^{-i\omega t} \left[a_{\omega\sigma}(0) - iJ \int_0^t dt' e^{i\omega t'} \right. \\ &\quad \left. \times \int d\omega' M_{\sigma\sigma'}(t') a_{\omega'\sigma'}(t') \right]. \end{aligned} \quad (\text{B1})$$

Transforming (B1) to the coordinate representation, we find

$$\begin{aligned} a_\sigma(x, t) &= a_\sigma(x - t, 0) - 2\pi i J \Theta(x) \Theta(t - x) \\ &\quad \times \sum_{\sigma'} M_{\sigma\sigma'}(t - x) a_{\sigma'}(0, t - x). \end{aligned} \quad (\text{B2})$$

Setting $x = 0$ and assuming $t > 0$, we obtain

$$a_\sigma(0, t) = \sum_{\sigma'} [1 + i\pi J M(t)]_{\sigma\sigma'}^{-1} a_{\sigma'}(-t, 0). \quad (\text{B3})$$

Noticing that

$$\sum_{\sigma'} M_{\sigma\sigma'}(t) M_{\sigma'\sigma''}(t) = -M_{\sigma\sigma''}(t), \quad (\text{B4})$$

we can express (B3) as

$$a_\sigma(0, t) = \sum_{\sigma'} \left[1 - \frac{i\pi J}{1 - i\pi J} M(t) \right]_{\sigma\sigma'} a_{\sigma'}(-t, 0). \quad (\text{B5})$$

Substituting this result into (B2) and considering $t > x > 0$, we obtain

$$a_\sigma(x, t) = \sum_{\sigma'} [1 + (1 - e^{i\phi}) M(t - x)]_{\sigma\sigma'} a_{\sigma'}(x - t, 0), \quad (\text{B6})$$

where $e^{i\phi} = \frac{1+i\pi J}{1-i\pi J}$.

The equation of motion for the spin operators $S^i(t)$ reads

$$\begin{aligned} \frac{d}{dt} S^i(t) &= 2\pi J \epsilon_{ijk} \sum_{\sigma, \sigma'} a_{\sigma\sigma'}^\dagger(0, t) \frac{\sigma_{\sigma\sigma'}^j}{2} S^k(t) a_{\sigma\sigma'}(0, t) \\ &\quad + \Delta \epsilon_{izk} S^k(t). \end{aligned} \quad (\text{B7})$$

Substituting (B5) into (B7), we obtain Eq. (14).

APPENDIX C: EVALUATION OF POLARIZATION UNRESOLVED SPECTRAL FUNCTION

The polarization unresolved correlation function is defined in (26). In the stationary limit, its Fourier transform

$$\tilde{C}^0(\omega) = 2 \operatorname{Re} \int_0^\infty d\tau e^{-i\omega\tau} C^0(\tau) \quad (\text{C1})$$

defines the power spectrum.

Defining the spin correlators $C^{ij}(\tau) = \langle S^i(t + \tau)S^j(t) \rangle$, we establish equations for them with help of (14) and (B5)

$$\begin{aligned} \frac{d}{d\tau} C^{ij}(\tau) &= \Omega \epsilon_{ilk} n_h^l C^{kj}(\tau) - \Gamma \left[C^{ij}(\tau) - \frac{n_{cl}^i \langle S^j \rangle_{st}}{2} \right] + 2\pi J \cos^2 \frac{\phi}{2} \sum_{\sigma, \sigma'} \epsilon_{ilk} \langle a_{\sigma}^{\dagger}(-t_{\tau}, 0) \frac{\sigma_{\sigma\sigma'}^l}{2} S^k(t_{\tau}) [a_{\sigma'}(-t_{\tau}, 0), S^j(t)] \rangle \\ &+ \frac{\pi J \sin \phi}{2} \sum_{\sigma, \sigma'} \langle a_{\sigma}^{\dagger}(-t_{\tau}, 0) \left[\frac{\sigma_{\sigma\sigma'}^i}{2} - \delta_{\sigma\sigma'} S^i(t_{\tau}) \right] [a_{\sigma'}(-t_{\tau}, 0), S^j(t)] \rangle, \end{aligned} \quad (C2)$$

where $t_{\tau} = t + \tau$.

Let us consider the commutators appearing in the above relation

$$\begin{aligned} [a_{\sigma}(-t_{\tau}, 0), S^i(t)] &= \int \frac{d\omega}{\sqrt{2\pi}} e^{-i\omega t_{\tau}} [a_{\omega\sigma}(0), S^i(t)] \\ &= iJ \int_0^t dt' \int \frac{d\omega d\omega'}{\sqrt{2\pi}} e^{i\omega(t'-t_{\tau})} [M_{\sigma\sigma'}(t') a_{\omega'\sigma'}(t'), S^i(t)] \\ &= \sqrt{2\pi} iJ \int_0^t dt' \delta(t' - t_{\tau}) \int d\omega' [M_{\sigma\sigma'}(t') a_{\omega'\sigma'}(t'), S^i(t)] \\ &= 2\pi iJ \Theta(-\tau) [M_{\sigma\sigma'}(t_{\tau}) a_{\sigma'}(0, t_{\tau}), S^i(t)], \end{aligned} \quad (C3)$$

where we have used (B1) and the commutation of the Heisenberg operators at equal time arguments, $[a_{\omega\sigma}(t), S^i(t)] = 0$, in the second step.

For $\tau > 0$ it follows

$$[a_{\sigma}(-t_{\tau}, 0), S^i(t)] = 0 \quad (C4)$$

and hence

$$\frac{d}{d\tau} C^{ij}(\tau) = \Omega \epsilon_{ilk} n_h^l C^{kj}(\tau) - \Gamma \left[C^{ij}(\tau) - \frac{n_{cl}^i \langle S^j \rangle_{st}}{2} \right]. \quad (C5)$$

Defining

$$A(\tau) = \langle \mathbf{S}(t + \tau) \cdot \mathbf{S}(t) \rangle = C^{ii}(\tau), \quad (C6)$$

$$\begin{aligned} B_{cl}(\tau) &= \mathbf{n}_{cl} \cdot \langle \mathbf{S}(t + \tau) \times \mathbf{S}(t) \rangle \\ &= \epsilon_{ijk} n_{cl}^k C^{ij}(\tau), \end{aligned} \quad (C7)$$

$$B_h(\tau) = \mathbf{n}_h \cdot \langle \mathbf{S}(t + \tau) \times \mathbf{S}(t) \rangle = \epsilon_{ijk} n_h^k C^{ij}(\tau), \quad (C8)$$

$$\begin{aligned} C_{cl,h}(\tau) &= \langle (\mathbf{n}_{cl} \cdot \mathbf{S}(t + \tau)) (\mathbf{n}_h \cdot \mathbf{S}(t)) \rangle \\ &= n_{cl}^i n_h^j C^{ij}(\tau), \end{aligned} \quad (C9)$$

$$\begin{aligned} C_{h,h}(\tau) &= \langle (\mathbf{n}_h \cdot \mathbf{S}(t + \tau)) (\mathbf{n}_h \cdot \mathbf{S}(t)) \rangle \\ &= n_h^i n_h^j C^{ij}(\tau), \end{aligned} \quad (C10)$$

$$\begin{aligned} D(\tau) &= \langle (\mathbf{n}_{cl} \cdot (\mathbf{n}_h \times \mathbf{S}(t + \tau))) (\mathbf{n}_h \cdot \mathbf{S}(t)) \rangle \\ &= \epsilon_{ikl} n_{cl}^k n_h^l n_h^j C^{ij}(\tau), \end{aligned} \quad (C11)$$

we derive the following equations:

$$\frac{d}{d\tau} A(\tau) = \Omega B_h(\tau) - \Gamma \left[A(\tau) - \frac{1}{4} \frac{1 + \lambda^2 \cos^2 \psi}{1 + \lambda^2} \right], \quad (C12)$$

$$\frac{d}{d\tau} B_{cl}(\tau) = \Omega [C_{cl,h}(\tau) - \cos \psi A(\tau)] - \Gamma B_{cl}(\tau), \quad (C13)$$

$$\frac{d}{d\tau} B_h(\tau) = \Omega [C_{h,h}(\tau) - A(\tau)] - \Gamma \left[B_h(\tau) - \frac{1}{4} \frac{\lambda \sin^2 \psi}{1 + \lambda^2} \right], \quad (C14)$$

$$\frac{d}{d\tau} C_{cl,h}(\tau) = \Omega D(\tau) - \Gamma \left[C_{cl,h}(\tau) - \frac{\cos \psi}{4} \right], \quad (C15)$$

$$\frac{d}{d\tau} C_{h,h}(\tau) = -\Gamma \left[C_{h,h}(\tau) - \frac{\cos^2 \psi}{4} \right], \quad (C16)$$

$$\frac{d}{d\tau} D(\tau) = \Omega [\cos \psi C_{h,h}(\tau) - C_{cl,h}(\tau)] - \Gamma D(\tau), \quad (C17)$$

with initial conditions specified by

$$A(0) = \frac{3}{4}, \quad (C18)$$

$$B_{cl}(0) = \frac{i}{2} \frac{1 + \lambda^2 \cos^2 \psi}{1 + \lambda^2}, \quad (C19)$$

$$B_h(0) = \frac{i}{2} \cos \psi, \quad (C20)$$

$$C_{cl,h}(0) = \frac{\cos \psi}{4} - \frac{i}{4} \frac{\lambda \sin^2 \psi}{1 + \lambda^2}, \quad (C21)$$

$$C_{h,h}(0) = \frac{1}{4}, \quad (C22)$$

$$D(0) = -\frac{i}{4} \frac{\sin^2 \psi}{1 + \lambda^2}. \quad (C23)$$

The solution of $C_{h,h}(\tau)$ can easily be found:

$$C_{h,h}(\tau) = \frac{1}{4} (\cos^2 \psi + \sin^2 \psi e^{-\Gamma\tau}). \quad (C24)$$

Using this result, we find

$$C_{cl,h}(\tau) = \frac{\cos \psi}{4} \left(\frac{1 + \lambda^2 \cos^2 \psi}{1 + \lambda^2} + \sin^2 \psi e^{-\Gamma\tau} \right) - \frac{i \sin^2 \psi}{4} \left(\cos^2 \frac{\psi}{2} \frac{e^{-(\Gamma-i\Omega)\tau}}{\lambda + i} + \sin^2 \frac{\psi}{2} \frac{e^{-(\Gamma+i\Omega)\tau}}{\lambda - i} \right), \quad (C25)$$

$$D(\tau) = \frac{\sin^2 \psi}{4} \left(\cos^2 \frac{\psi}{2} \frac{e^{-(\Gamma-i\Omega)\tau}}{\lambda + i} - \sin^2 \frac{\psi}{2} \frac{e^{-(\Gamma+i\Omega)\tau}}{\lambda - i} - \frac{\lambda \cos \psi}{1 + \lambda^2} \right), \quad (C26)$$

$$A(\tau) = \frac{1}{4} \frac{1 + \lambda^2 \cos^2 \psi}{1 + \lambda^2} + \frac{\sin^2 \psi}{4} e^{-\Gamma\tau} + \frac{1}{2} \left(\cos^2 \frac{\psi}{2} - \frac{1}{4} \frac{\sin^2 \psi}{1 + \lambda^2} \right) e^{-(\Gamma-i\Omega)\tau} + \frac{1}{2} \left(\sin^2 \frac{\psi}{2} - \frac{1}{4} \frac{\sin^2 \psi}{1 + \lambda^2} \right) e^{-(\Gamma+i\Omega)\tau}, \quad (\text{C27})$$

$$B_h(\tau) = \frac{i}{2} \left(\cos^2 \frac{\psi}{2} - \frac{1}{4} \frac{\sin^2 \psi}{1 + \lambda^2} \right) e^{-(\Gamma-i\Omega)\tau} - \frac{i}{2} \left(\sin^2 \frac{\psi}{2} - \frac{1}{4} \frac{\sin^2 \psi}{1 + \lambda^2} \right) e^{-(\Gamma+i\Omega)\tau}. \quad (\text{C28})$$

This information allows us to find

$$B_{cl}(\tau) = \frac{i}{4} \frac{\sin^2 \psi}{1 + \lambda^2} (1 - i\lambda \cos \psi) e^{-\Gamma\tau} + i \left[\cos^2 \frac{\psi}{2} \left(\frac{\sin^2 \psi}{4} \frac{1}{1 - i\lambda} + \frac{\cos \psi}{2} \right) - \frac{1}{8} \frac{\cos \psi \sin^2 \psi}{1 + \lambda^2} \right] e^{-(\Gamma-i\Omega)\tau} \\ + i \left[\sin^2 \frac{\psi}{2} \left(\frac{\sin^2 \psi}{4} \frac{1}{1 + i\lambda} - \frac{\cos \psi}{2} \right) + \frac{1}{8} \frac{\cos \psi \sin^2 \psi}{1 + \lambda^2} \right] e^{-(\Gamma+i\Omega)\tau} \quad (\text{C29})$$

and

$$A(\tau) + iB_{cl}(\tau) = \frac{1}{4} \frac{1 + \lambda^2 \cos^2 \psi}{1 + \lambda^2} + \frac{1}{4} \frac{\lambda \sin^2 \psi}{1 + \lambda^2} (\lambda + i \cos \psi) e^{-\Gamma\tau} + \frac{1}{4} \frac{\lambda \sin^2 \psi}{1 + \lambda^2} \left(\lambda - i \cos^2 \frac{\psi}{2} \right) e^{-(\Gamma-i\Omega)\tau} \\ + \frac{1}{4} \frac{\lambda \sin^2 \psi}{1 + \lambda^2} \left(\lambda + i \sin^2 \frac{\psi}{2} \right) e^{-(\Gamma+i\Omega)\tau}. \quad (\text{C30})$$

Combining (26), (C1), and (C30), we obtain the polarization unresolved power spectrum (32).

APPENDIX D: EVALUATION OF POLARIZATION RESOLVED SPECTRAL FUNCTION

To evaluate the polarization resolved correlation function (36), we additionally introduce

$$\mathbf{A}_L(\tau) \equiv \langle (\mathbf{n}_{cl} \cdot \mathbf{S}(t + \tau)) \mathbf{S}(t) \rangle, \quad (\text{D1})$$

$$\mathbf{A}_R(\tau) \equiv \langle \mathbf{S}(t + \tau) (\mathbf{n}_{cl} \cdot \mathbf{S}(t)) \rangle, \quad (\text{D2})$$

$$\mathbf{B}_g(\tau) \equiv \langle \mathbf{S}(t + \tau) \times \mathbf{S}(t) \rangle. \quad (\text{D3})$$

Assuming $\mathbf{n}_{cl} \nparallel \mathbf{n}_h$, we expand (D1)–(D3) in the (nonorthogonal) basis $\{\mathbf{n}_{cl}, \mathbf{n}_h, \mathbf{n}_{cl} \times \mathbf{n}_h\}$:

$$\mathbf{A}_L(\tau) = \frac{C_{cl,cl}(\tau) - \cos \psi C_{cl,h}(\tau)}{\sin^2 \psi} \mathbf{n}_{cl} \\ + \frac{C_{cl,h}(\tau) - \cos \psi C_{cl,cl}(\tau)}{\sin^2 \psi} \mathbf{n}_h + \frac{E_R(\tau)}{\sin^2 \psi} \mathbf{n}_{cl} \times \mathbf{n}_h, \quad (\text{D4})$$

$$\mathbf{A}_R(\tau) = \frac{C_{cl,cl}(\tau) - \cos \psi C_{h,cl}(\tau)}{\sin^2 \psi} \mathbf{n}_{cl} \\ + \frac{C_{h,cl}(\tau) - \cos \psi C_{cl,cl}(\tau)}{\sin^2 \psi} \mathbf{n}_h + \frac{E_L(\tau)}{\sin^2 \psi} \mathbf{n}_{cl} \times \mathbf{n}_h, \quad (\text{D5})$$

$$\mathbf{B}_g(\tau) = \frac{B_{cl}(\tau) - \cos \psi B_h(\tau)}{\sin^2 \psi} \mathbf{n}_{cl} \\ + \frac{B_h(\tau) - \cos \psi B_{cl}(\tau)}{\sin^2 \psi} \mathbf{n}_h \\ + \frac{C_{cl,h}(\tau) - C_{h,cl}(\tau)}{\sin^2 \psi} \mathbf{n}_{cl} \times \mathbf{n}_h, \quad (\text{D6})$$

where

$$C_{cl,cl}(\tau) = \langle (\mathbf{n}_{cl} \cdot \mathbf{S}(t + \tau)) (\mathbf{n}_{cl} \cdot \mathbf{S}(t)) \rangle \\ = n_{cl}^i n_{cl}^j C_{ij}(\tau), \quad (\text{D7})$$

$$C_{h,cl}(\tau) = \langle (\mathbf{n}_h \cdot \mathbf{S}(t + \tau)) (\mathbf{n}_{cl} \cdot \mathbf{S}(t)) \rangle \\ = n_h^i n_{cl}^j C_{ij}(\tau), \quad (\text{D8})$$

$$E_R(\tau) = \langle (\mathbf{n}_{cl} \cdot \mathbf{S}(t + \tau)) \mathbf{n}_{cl} \cdot (\mathbf{n}_h \times \mathbf{S}(t)) \rangle \\ = \epsilon_{jkl} n_{cl}^k n_{cl}^i n_h^l C_{ij}(\tau), \quad (\text{D9})$$

$$E_L(\tau) = \langle \mathbf{n}_{cl} \cdot (\mathbf{n}_h \times \mathbf{S}(t + \tau)) (\mathbf{n}_{cl} \cdot \mathbf{S}(t)) \rangle \\ = \epsilon_{ikl} n_{cl}^k n_{cl}^j n_h^l C_{ij}(\tau), \quad (\text{D10})$$

$$F(\tau) = \langle ((\mathbf{n}_{cl} \times \mathbf{n}_h) \cdot \mathbf{S}(t + \tau)) ((\mathbf{n}_{cl} \times \mathbf{n}_h) \cdot \mathbf{S}(t)) \rangle \\ = \epsilon_{inm} \epsilon_{jkl} n_{cl}^k n_{cl}^n n_h^l n_h^m C_{ij}(\tau), \quad (\text{D11})$$

$$\bar{F}(\tau) = \langle (\mathbf{n}_h \cdot \mathbf{S}(t + \tau)) ((\mathbf{n}_{cl} \times \mathbf{n}_h) \cdot \mathbf{S}(t)) \rangle \\ = \epsilon_{jkl} n_{cl}^k n_h^l n_h^i C_{ij}(\tau). \quad (\text{D12})$$

From (C5) we derive the following equations at $\tau > 0$:

$$\frac{d}{d\tau} C_{cl,cl}(\tau) = \Omega E_L(\tau) - \Gamma \left[C_{cl,cl}(\tau) - \frac{1}{4} \frac{1 + \lambda^2 \cos^2 \psi}{1 + \lambda^2} \right], \quad (\text{D13})$$

$$\frac{d}{d\tau} C_{h,cl}(\tau) = -\Gamma \left[C_{h,cl}(\tau) - \frac{\cos \psi}{4} \frac{1 + \lambda^2 \cos^2 \psi}{1 + \lambda^2} \right], \quad (\text{D14})$$

$$\frac{d}{d\tau} E_R(\tau) = \Omega F(\tau) - \Gamma \left[E_R(\tau) + \frac{1}{4} \frac{\lambda \sin^2 \psi}{1 + \lambda^2} \right], \quad (\text{D15})$$

$$\frac{d}{d\tau} F(\tau) = \Omega [\cos \psi \bar{F}(\tau) - E_R(\tau)] - \Gamma F(\tau), \quad (\text{D16})$$

$$\frac{d}{d\tau} \bar{F}(\tau) = -\Gamma \left[\bar{F}(\tau) + \frac{\cos \psi}{4} \frac{\lambda \sin^2 \psi}{1 + \lambda^2} \right], \quad (\text{D17})$$

$$\frac{d}{d\tau} E_L(\tau) = \Omega [\cos \psi C_{h,cl}(\tau) - C_{cl,cl}(\tau)] - \Gamma E_L(\tau), \quad (\text{D18})$$

with the initial conditions

$$C_{cl,cl}(0) = \frac{1}{4}, \quad (D19)$$

$$C_{h,cl}(0) = \frac{\cos \psi}{4} + \frac{i \lambda \sin^2 \psi}{4(1 + \lambda^2)}, \quad (D20)$$

$$E_R(0) = -i \frac{\cos \psi}{4} \frac{\lambda^2 \sin^2 \psi}{1 + \lambda^2}, \quad (D21)$$

$$F(0) = \frac{\sin^2 \psi}{4}, \quad (D22)$$

$$\bar{F}(0) = \frac{i \sin^2 \psi}{4(1 + \lambda^2)}, \quad (D23)$$

$$E_L(0) = i \frac{\cos \psi}{4} \frac{\lambda^2 \sin^2 \psi}{1 + \lambda^2}. \quad (D24)$$

We can immediately solve (D14) and find

$$C_{h,cl}(\tau) = \frac{\cos \psi}{4} \frac{1 + \lambda^2 \cos^2 \psi}{1 + \lambda^2} + \frac{1}{4} \frac{\lambda \sin^2 \psi}{1 + \lambda^2} (\lambda \cos \psi + i) e^{-\Gamma \tau}. \quad (D25)$$

This result allows us to solve (D13) and (D18) in the next step. Thus, we obtain

$$\begin{aligned} C_{cl,cl}(\tau) &= \frac{1}{4} \left(\frac{1 + \lambda^2 \cos^2 \psi}{1 + \lambda^2} \right)^2 + \frac{\cos \psi}{4} \frac{\lambda \sin^2 \psi}{1 + \lambda^2} (\lambda \cos \psi + i) e^{-\Gamma \tau} \\ &+ \frac{1}{8} \frac{\lambda \sin^2 \psi}{1 + \lambda^2} \left[\frac{\lambda \sin^2 \psi}{1 + \lambda^2} + \lambda(1 + \cos \psi) - i \left(\cos \psi + \frac{1 + \lambda^2 \cos^2 \psi}{1 + \lambda^2} \right) \right] e^{-(\Gamma - i\Omega)\tau} \\ &+ \frac{1}{8} \frac{\lambda \sin^2 \psi}{1 + \lambda^2} \left[\frac{\lambda \sin^2 \psi}{1 + \lambda^2} + \lambda(1 - \cos \psi) - i \left(\cos \psi - \frac{1 + \lambda^2 \cos^2 \psi}{1 + \lambda^2} \right) \right] e^{-(\Gamma + i\Omega)\tau}, \end{aligned} \quad (D26)$$

$$\begin{aligned} E_L(\tau) &= -\lambda \frac{\sin^2 \psi}{4} \frac{1 + \lambda^2 \cos^2 \psi}{(1 + \lambda^2)^2} + \frac{i}{8} \frac{\lambda \sin^2 \psi}{1 + \lambda^2} \left[\frac{\lambda \sin^2 \psi}{1 + \lambda^2} + \lambda(1 + \cos \psi) - i \left(\cos \psi + \frac{1 + \lambda^2 \cos^2 \psi}{1 + \lambda^2} \right) \right] e^{-(\Gamma - i\Omega)\tau} \\ &- \frac{i}{8} \frac{\lambda \sin^2 \psi}{1 + \lambda^2} \left[\frac{\lambda \sin^2 \psi}{1 + \lambda^2} + \lambda(1 - \cos \psi) - i \left(\cos \psi - \frac{1 + \lambda^2 \cos^2 \psi}{1 + \lambda^2} \right) \right] e^{-(\Gamma + i\Omega)\tau}. \end{aligned} \quad (D27)$$

Similarly, from (D17) we find

$$\bar{F}(\tau) = \frac{1}{4} \frac{\sin^2 \psi}{1 + \lambda^2} [-\lambda \cos \psi + (i + \lambda \cos \psi) e^{-\Gamma \tau}], \quad (D28)$$

which enables us to solve (D15) and (D16). Thus, we find

$$F(\tau) = \frac{1}{4} \frac{\lambda^2 \sin^4 \psi}{(1 + \lambda^2)^2} + \frac{\sin^2 \psi}{8} \left(1 + \cos \psi + \frac{i \lambda}{1 - i \lambda} \frac{\sin^2 \psi}{1 + \lambda^2} \right) e^{-(\Gamma - i\Omega)\tau} + \frac{\sin^2 \psi}{8} \left(1 - \cos \psi - \frac{i \lambda}{1 + i \lambda} \frac{\sin^2 \psi}{1 + \lambda^2} \right) e^{-(\Gamma + i\Omega)\tau}, \quad (D29)$$

and

$$\begin{aligned} E_R(\tau) &= -\frac{1}{4} \frac{\lambda \sin^2 \psi (1 + \lambda^2 \cos^2 \psi)}{(1 + \lambda^2)^2} + \frac{1}{4} \frac{\cos \psi \sin^2 \psi}{1 + \lambda^2} (i + \lambda \cos \psi) e^{-\Gamma \tau} - \frac{i \sin^2 \psi}{8} \left(1 + \cos \psi + \frac{i \lambda}{1 - i \lambda} \frac{\sin^2 \psi}{1 + \lambda^2} \right) e^{-(\Gamma - i\Omega)\tau} \\ &+ \frac{i \sin^2 \psi}{8} \left(1 - \cos \psi - \frac{i \lambda}{1 + i \lambda} \frac{\sin^2 \psi}{1 + \lambda^2} \right) e^{-(\Gamma + i\Omega)\tau}. \end{aligned} \quad (D30)$$

Collecting all contributions, we obtain

$$\mathbf{A}_R(\tau) + \mathbf{A}_L(\tau) - \mathbf{n}_{cl} \mathbf{A}(\tau) - i \mathbf{B}_g(\tau) = a \mathbf{n}_{cl} + b \mathbf{n}_h + c \mathbf{n}_{cl} \times \mathbf{n}_h, \quad (D31)$$

where the coefficients a, b, c are given by

$$a = \frac{1}{4} \frac{(1 - \lambda^2)(1 + \lambda^2 \cos^2 \psi)}{(1 + \lambda^2)^2} - \frac{1}{4} \frac{\lambda^2 \sin^2 \psi}{1 + \lambda^2} e^{-\Gamma \tau} - \frac{i}{8} \frac{\lambda \sin^2 \psi}{1 + \lambda^2} \left[\frac{1 + i\lambda}{1 - i\lambda} e^{-(\Gamma - i\Omega)\tau} - \frac{1 - i\lambda}{1 + i\lambda} e^{-(\Gamma + i\Omega)\tau} \right], \quad (\text{D32})$$

$$b = \frac{\lambda^2 \cos \psi}{2} \frac{1 + \lambda^2 \cos^2 \psi}{(1 + \lambda^2)^2} + \frac{1}{4} \frac{\lambda \sin^2 \psi}{1 + \lambda^2} (i + 2\lambda \cos \psi) e^{-\Gamma \tau} + \frac{1}{8} \frac{\lambda \sin^2 \psi}{1 + \lambda^2} \left[\left(2\lambda - 2\lambda \frac{\cos \psi}{1 - i\lambda} - i \right) e^{-(\Gamma - i\Omega)\tau} - \left(2\lambda + 2\lambda \frac{\cos \psi}{1 + i\lambda} + i \right) e^{-(\Gamma + i\Omega)\tau} \right], \quad (\text{D33})$$

$$c = -\frac{\lambda}{2} \frac{1 + \lambda^2 \cos^2 \psi}{(1 + \lambda^2)^2} - \frac{1}{4} \frac{\lambda \sin^2 \psi}{1 + \lambda^2} e^{-\Gamma \tau} + \frac{1}{8} \frac{\lambda \sin^2 \psi}{1 + \lambda^2} \left[\frac{1 + i\lambda}{1 - i\lambda} e^{-(\Gamma - i\Omega)\tau} + \frac{1 - i\lambda}{1 + i\lambda} e^{-(\Gamma + i\Omega)\tau} \right]. \quad (\text{D34})$$

The Fourier transform of (D31) leads us to (41).

APPENDIX E: COMPUTATION OF $g^{(2)}$ FUNCTION

To obtain expression for the second-order correlation functions defined in (43) and (44), we introduce the quantities

$$\mathbf{K}_m(\tau) = \sum_{\bar{\sigma}', \bar{\sigma}} \sum_{\sigma', \sigma} \left(\mathbf{m} \cdot \frac{\boldsymbol{\sigma}_{\sigma'\sigma}}{2} \right) \frac{\alpha_{\bar{\sigma}'}^* \alpha_{\bar{\sigma}}}{L} \langle [\delta_{\bar{\sigma}'\sigma'} + (1 - e^{-i\phi}) M_{\bar{\sigma}'\sigma'}(t)] \mathbf{S}(t + \tau) [\delta_{\sigma\bar{\sigma}} + (1 - e^{i\phi}) M_{\sigma\bar{\sigma}}(t)] \rangle, \quad (\text{E1})$$

$$\mathbf{K}_0(\tau) = \sum_{\bar{\sigma}', \bar{\sigma}} \sum_{\sigma} \frac{\alpha_{\bar{\sigma}'}^* \alpha_{\bar{\sigma}}}{L} \langle [\delta_{\bar{\sigma}'\sigma} + (1 - e^{-i\phi}) M_{\bar{\sigma}'\sigma}(t)] \mathbf{S}(t + \tau) [\delta_{\sigma\bar{\sigma}} + (1 - e^{i\phi}) M_{\sigma\bar{\sigma}}(t)] \rangle, \quad (\text{E2})$$

and using (14) we establish that they obey the equations

$$\frac{d}{d\tau} \mathbf{K}_m(\tau) = \Omega \mathbf{n}_h \times \mathbf{K}_m(\tau) - \Gamma [\mathbf{K}_m(\tau) - \frac{A_m}{2} \mathbf{n}_{cl}], \quad (\text{E3})$$

$$\frac{d}{d\tau} \mathbf{K}_0(\tau) = \Omega \mathbf{n}_h \times \mathbf{K}_0(\tau) - \Gamma \left[\mathbf{K}_0(\tau) - \frac{A_0}{2} \mathbf{n}_{cl} \right], \quad (\text{E4})$$

where

$$A_m = \sum_{\bar{\sigma}', \bar{\sigma}} \sum_{\sigma', \sigma} \left(\mathbf{m} \cdot \frac{\boldsymbol{\sigma}_{\sigma'\sigma}}{2} \right) \frac{\alpha_{\bar{\sigma}'}^* \alpha_{\bar{\sigma}}}{L} \langle [\delta_{\bar{\sigma}'\sigma'} + (1 - e^{-i\phi}) M_{\bar{\sigma}'\sigma'}(t)] [\delta_{\sigma\bar{\sigma}} + (1 - e^{i\phi}) M_{\sigma\bar{\sigma}}(t)] \rangle = \mathbf{m} \cdot \mathbf{C}_s(0), \quad (\text{E5})$$

$$A_0 = \sum_{\bar{\sigma}', \bar{\sigma}} \sum_{\sigma} \frac{\alpha_{\bar{\sigma}'}^* \alpha_{\bar{\sigma}}}{L} \langle [\delta_{\bar{\sigma}'\sigma} + (1 - e^{-i\phi}) M_{\bar{\sigma}'\sigma}(t)] [\delta_{\sigma\bar{\sigma}} + (1 - e^{i\phi}) M_{\sigma\bar{\sigma}}(t)] \rangle = f. \quad (\text{E6})$$

After rescaling $\mathbf{k}_m(\tau) = \frac{\mathbf{K}_m(\tau)}{A_m}$ and $\mathbf{k}_0(\tau) = \frac{\mathbf{K}_0(\tau)}{f}$, we obtain the equations quoted in Sec. IV.

-
- [1] A. D. Greentree, C. Tahan, J. H. Cole, and L. C. L. Hollenberg, Quantum phase transitions of light, *Nat. Phys.* **2**, 856 (2006).
- [2] M. J. Hartmann, F. G. S. L. Brandao, and M. B. Plenio, Strongly interacting polaritons in coupled arrays of cavities, *Nat. Phys.* **2**, 849 (2006).
- [3] D. G. Angelakis, M. F. Santos, and S. Bose, Photon-blockade-induced Mott transitions and XY spin models in coupled cavity arrays, *Phys. Rev. A* **76**, 031805 (2007).
- [4] D. E. Chang, V. Gritsev, G. Morigi, V. Vuletic, M. D. Lukin, and E. A. Demler, Crystallization of strongly interacting photons in a nonlinear optical fibre, *Nat. Phys.* **4**, 884 (2008).
- [5] I. Carusotto, D. Gerace, H. E. Tureci, S. De Liberato, C. Ciuti, and A. Imamoglu, Fermionized Photons in an Array of Driven Dissipative Nonlinear Cavities, *Phys. Rev. Lett.* **103**, 033601 (2009).
- [6] J. Klaers, J. Schmitt, F. Vewinger, and M. Weitz, Bose-Einstein condensation of photons in an optical microcavity, *Nature (London)* **468**, 545 (2010).
- [7] Z. Wang, Y. Chong, J. D. Joannopoulos, and M. Soljačić, Observation of unidirectional backscattering-immune topological electromagnetic states, *Nature (London)* **461**, 772 (2009).
- [8] A. B. Khanikaev, S. H. Mousavi, W.-K. Tse, M. Kargarian, A. H. MacDonald, and G. Shvets, Photonic topological insulators, *Nat. Mater.* **12**, 233 (2013).
- [9] M. Hafezi, E. A. Demler, M. D. Lukin, and J. M. Taylor, Robust optical delay lines with topological protection, *Nat. Phys.* **7**, 907 (2011).
- [10] I. Carusotto and C. Ciuti, Quantum fluids of light, *Rev. Mod. Phys.* **85**, 299 (2013).
- [11] C. Noh and D. G. Angelakis, Quantum simulations and many-body physics with light, *Rep. Prog. Phys.* **80**, 016401 (2016).

- [12] H. J. Kimble, The quantum internet, *Nature (London)* **453**, 1023 (2008).
- [13] Y. Chu and M. D. Lukin, *Quantum Optics with Nitrogen-Vacancy Centers in Diamond* (Oxford University Press, 2015).
- [14] P. Neumann *et al.*, Multipartate entanglement among single spins in diamond, *Science* **320**, 1326 (2008).
- [15] M. Ansmann, H. Wang, R. C. Bialczak, M. Hofheinz, E. Lucero, M. Neeley, A. D. O'Connell, D. Sank, M. Weides, J. Wenner, A. N. Cleland, and J. M. Martinis, Violation of Bell's inequality in Josephson phase qubits, *Nature (London)* **461**, 504 (2009).
- [16] F. Dolde, I. Jakobi, B. Naydenov, N. Zhao, S. Pezzagna, C. Trautmann, J. Meijer, P. Neumann, F. Jelezko, and J. Wrachtrup, Room-temperature entanglement between single defect spins in diamond, *Nat. Phys.* **9**, 139 (2013).
- [17] H. Bernien, B. Hensen, W. Pfaff, G. Koolstra, M. S. Blok, L. Robledo, T. H. Taminiu, M. Markham, D. J. Twitchen, L. Childress, and R. Hanson, Heralded entanglement between solid-state qubits separated by three meters, *Nature (London)* **497**, 86 (2013).
- [18] M. D. Lukin, Colloquium: Trapping and manipulating photon states in atomic ensembles, *Rev. Mod. Phys.* **75**, 457 (2003).
- [19] M. Fleischhauer, A. Imamoglu, and J. P. Marangos, Electromagnetically induced transparency: Optics in coherent media, *Rev. Mod. Phys.* **77**, 633 (2005).
- [20] G. Alzetta, A. Gozzini, L. Moi, and G. Orriols, An experimental method for the observation of r.f. transitions and laser beat resonances in oriented vapour, *Nuovo Cimento B* **36**, 5 (1976).
- [21] E. Arimondo and G. Orriols, Nonabsorbing atomic coherences by coherent two-photon transitions in a three level optical pumping, *Lett. Nuovo Cimento* (1971) **17**, 333 (1976).
- [22] H. R. Gray, R. M. Whitley, and C. R. Stroud, Jr., Coherent trapping of atomic populations, *Opt. Lett.* **3**, 218 (1978).
- [23] G. Orriols, Nonabsorption resonances by nonlinear coherent effects in a three-level system, *Nuovo Cimento B* **53**, 1 (1979).
- [24] E. Arimondo, Relaxation processes in coherent-population trapping, *Phys. Rev. A* **54**, 2216 (1996).
- [25] A. Aspect, E. Arimondo, R. Kaiser, N. Vansteenkiste, and C. Cohen-Tannoudji, Laser Cooling Below the one Photon Recoil Energy by Velocity-Selective Coherent Population Trapping, *Phys. Rev. Lett.* **61**, 826 (1988).
- [26] J. R. Kuklinski, U. Gaubatz, F. T. Hioe, and K. Bergmann, Adiabatic population transfer in a three-level system driven by delayed laser pulses, *Phys. Rev. A* **40**, 6741 (1989).
- [27] U. Gaubatz, P. Rudecki, S. Schiemann, and K. Bergmann, Population transfer between molecular levels by stimulated Raman scattering with partially overlapping pulses: A new concept and experimental results, *J. Chem. Phys.* **92**, 5363 (1990).
- [28] K. Bergmann, H. Theuer, and B. W. Shore, Coherent population transfer among quantum states of atoms and molecules, *Rev. Mod. Phys.* **70**, 1003 (1998).
- [29] N. V. Vitanov, M. Fleischhauer, B. W. Shore, and K. Bergmann, Coherent manipulation of atoms and molecules by sequential pulses, *Adv. At., Mol. Opt. Phys.* **46**, 55 (2001).
- [30] K. Bergmann, N. V. Vitanov, and B. W. Shore, Perspective: Stimulated Raman adiabatic passage: The status after 25 years, *J. Chem. Phys.* **142**, 170901 (2015).
- [31] S. H. Autler and C. H. Townes, Stark effect in rapidly varying fields, *Phys. Rev.* **100**, 703 (1955).
- [32] C. Cohen-Tannoudji, The Autler-Townes effect revisited, in *Amazing Light* (Springer, New York, 1996).
- [33] P. M. Anisimov, J. P. Dowling, and B. C. Sanders, Objectively Discerning Autler-Townes Splitting from Electromagnetically Induced Transparency, *Phys. Rev. Lett.* **107**, 163604 (2011).
- [34] C. Cohen-Tannoudji and S. Reynaud, Dressed-atom description of resonance fluorescence and absorption spectra of a multi-level atom in an intense laser beam, *J. Phys. B* **10**, 345 (1977).
- [35] R. M. Whitley and C. R. Stroud, Jr., Double optical resonance, *Phys. Rev. A* **14**, 1498 (1976).
- [36] B. Sobolewska, The fluorescence spectrum of a three-level atom in two-photon resonance with the laser field, *Opt. Commun.* **20**, 378 (1977).
- [37] C.-R. Fu, Y.-M. Zhang, and C. de Gong, Resonance fluorescence from a three-level system, *Phys. Rev. A* **45**, 505 (1992).
- [38] C. Mavroyannis, Resonance fluorescence spectrum of a three-level atom, *Opt. Commun.* **29**, 80 (1979).
- [39] C. Mavroyannis, Two-photon resonance fluorescence, *Opt. Commun.* **26**, 453 (1978).
- [40] M. Alexanian and S. K. Bose, Two-photon resonance fluorescence, *Phys. Rev. A* **74**, 063418 (2006).
- [41] S. K. Basu, T. Pramila, and D. Kanjilal, Dynamic Stark splitting in two-photon resonance fluorescence, *Opt. Commun.* **45**, 43 (1983).
- [42] A. N. Vamivakas, Y. Zhao, C.-Y. Lu, and M. Atatüre, Spin-resolved quantum-dot resonance fluorescence, *Nat. Phys.* **5**, 198 (2009).
- [43] S. E. Harris and L. V. Hau, Nonlinear Optics at Low Light Levels, *Phys. Rev. Lett.* **82**, 4611 (1999).
- [44] M. M. Kash, V. A. Sautenkov, A. S. Zibrov, L. Hollberg, G. R. Welch, M. D. Lukin, Y. Rostovtsev, E. S. Fry, and M. O. Scully, Ultraslow Group Velocity and Enhanced Nonlinear Optical Effects in a Coherently Driven Hot Atomic Gas, *Phys. Rev. Lett.* **82**, 5229 (1999).
- [45] H. Wang, D. Goorskey, and M. Xiao, Enhanced Kerr Nonlinearity via Atomic Coherence in a Three-Level Atomic System, *Phys. Rev. Lett.* **87**, 073601 (2001).
- [46] W. Denk, J. Strickler, and W. Webb, Two-photon laser scanning fluorescence microscopy, *Science* **248**, 73 (1990).
- [47] P. T. C. So, C. Y. Dong, B. R. Masters, and K. M. Berland, Two-photon excitation fluorescence microscopy, *Annu. Rev. Biomed. Eng.* **2**, 399 (2000).
- [48] D. Budker, W. Gawlik, D. F. Kimball, S. M. Rochester, V. V. Yashchuk, and A. Weis, Resonant nonlinear magneto-optical effects in atoms, *Rev. Mod. Phys.* **74**, 1153 (2002).
- [49] J. Kondo, Resistance minimum in dilute magnetic alloys, *Prog. Theor. Phys.* **32**, 37 (1964).
- [50] P. W. Anderson, Localized magnetic states in metals, *Phys. Rev.* **124**, 41 (1961).
- [51] S. M. Cronenwett, T. H. Oosterkamp, and L. P. Kouwenhoven, A tunable Kondo effect in quantum dots, *Science* **281**, 540 (1998).
- [52] L. I. Glazman and M. E. Raikh, Resonant Kondo transparency of a barrier with quasilocal impurity states, *JETP Lett.* **47**, 452 (1988).
- [53] A. LeClair, QED for a fibrillar medium of two-level atoms, *Phys. Rev. A* **56**, 782 (1997).
- [54] R. Konik and A. LeClair, The scattering theory of oscillator defects in an optical fiber, *Phys. Rev. B* **58**, 1872 (1998).

- [55] A. LeClair, F. Lesage, S. Lukyanov, and H. Saleur, The Maxwell-Bloch theory in quantum optics and the Kondo model, *Phys. Lett. A* **235**, 203 (1997).
- [56] A. LeClair, Eigenstates of the atom-field interaction and the binding of light in photonic crystals, *Ann. Phys.* **271**, 268 (1999).
- [57] K. Le Hur, Kondo resonance of a microwave photon, *Phys. Rev. B* **85**, 140506(R) (2012).
- [58] K. Le Hur, Quantum phase transitions in spin-boson systems: Dissipation and light phenomena, in *Understanding Quantum Phase Transitions*, edited by L. D. Carr (Taylor and Francis, Boca Raton, FL, 2010).
- [59] H. E. Türeci, M. Hanl, M. Claassen, A. Weichselbaum, T. Hecht, B. Braunecker, A. Govorov, L. Glazman, A. Imamoglu, and J. von Delft, Many-Body Dynamics of Exciton Creation in a Quantum Dot by Optical Absorption: A Quantum Quench Towards Kondo Correlations, *Phys. Rev. Lett.* **106**, 107402 (2011).
- [60] B. Sbierski, M. Hanl, A. Weichselbaum, H. E. Türeci, M. Goldstein, L. I. Glazman, J. von Delft, and A. Imamoglu, Proposed Rabi-Kondo Correlated State in a Laser-Driven Semiconductor Quantum Dot, *Phys. Rev. Lett.* **111**, 157402 (2013).
- [61] J. R. Schrieffer and P. A. Wolff, Relation between the Anderson and Kondo Hamiltonians, *Phys. Rev.* **149**, 491 (1966).
- [62] R. C. Jones, A new calculus for the treatment of optical systems: description and discussion of the calculus, *J. Opt. Soc. Am.* **31**, 488 (1941).
- [63] P. Zoller and C. Gardiner, *Quantum Noise* (Springer-Verlag, New York, 2004).